buildings

Article

Post-Fire Mechanical Properties of Half-Grouted Sleeve Connectors with Grouting Defects

Shouying Hu [1], Shan Jiang [2], Dong Chen [2,*], Haoran Li [2] and Tao Xu [3]

1 A+E Design Co., Ltd., Shenzhen 518031, China; hushouying@ae-design.cn
2 Anhui BIM Engineering Center, Anhui Jianzhu University, Hefei 230601, China; jiangshan1017@stu.ahjzu.edu.cn (S.J.); lihaoran@stu.ahjzu.edu.cn (H.L.)
3 China Construction First Group the Fifth Construction Co., Ltd., Beijing 100024, China; jiaodaowei@cscec.com
* Correspondence: chendong@ahjzu.edu.cn

Abstract: Half-grouted sleeve connectors are a primary method for connecting rebar in prefabricated concrete structures. However, due to limitations in the construction environment, all kinds of grouting defects are inevitable, especially grouting voids. Additionally, fire disasters, among the most common types of disasters, significantly threaten the structural performance and safety of these prefabricated structures. Therefore, it is imperative to determine the mechanical properties of half-grouted sleeve connectors with grouting voids after high temperatures. This study designed and prepared 48 groups of half-grouted sleeve specimens with different grouting voids and defect locations. These specimens were heated to the specified temperature (25 °C, 200 °C, 300 °C, 400 °C, 500 °C, 600 °C), followed by unidirectional tensile testing after natural cooling. The experimental results showed that rebar fracture failure and rebar pulled-out failure were the failure modes of specimens. With the increase in temperature, bearing capacity, safety factor and ductility coefficient of specimens all decreased. When the temperature was lower than 400 °C, the specimen with void length less than twice the diameter of the rebar (i.e., 2d) had sufficient connection performance. For specimens with the same total void lengths, the bearing capacity of discrete voids is lower than concentrate voids at the same temperature. The load-displacement curve, safety coefficient, ductility coefficient and grey correlation degree of half-grouted sleeve specimens with grouting voids at different temperatures are analyzed and discussed, and the bond stress slip constitutive model is given. Grouting defects have greater influence on specimens after grey correlation analysis. Findings from this study provide valuable references for the safety performance evaluation of prefabricated structures with half-grouted sleeve connectors after exposure to fire.

Keywords: prefabricated structure; half-grouted sleeve connectors; fire; grouting defects; mechanical properties

Citation: Hu, S.; Jiang, S.; Chen, D.; Li, H.; Xu, T. Post-Fire Mechanical Properties of Half-Grouted Sleeve Connectors with Grouting Defects. *Buildings* **2024**, *14*, 1434. https://doi.org/10.3390/buildings14051434

Academic Editor: Mohamed K. Ismail

Received: 28 April 2024
Revised: 8 May 2024
Accepted: 12 May 2024
Published: 16 May 2024

1. Introduction

Prefabricated concrete structures offer significant advantages over cast-in-place concrete structures, including energy savings, environmental protection, shorter construction periods and lower engineering costs. Currently, the safety of prefabricated concrete structures relies on the performance of their joints [1,2]. The grouted sleeve serves as the primary connection method for prefabricated components and can be classified into two types: half-grouted sleeve and full-grouted sleeve. In the half-grouted sleeve, one end is connected to the rebar using threads, while the other end is inserted into the inner cavity and secured through the injection of high-strength grout [3]. This connection method is primarily utilized in shear walls and precast reinforced concrete structures, as depicted in Figure 1.

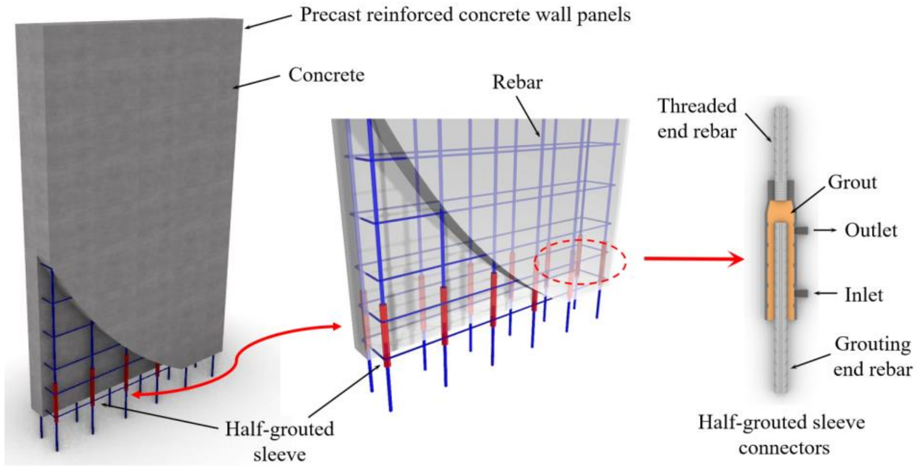

Figure 1. Precast reinforced concrete wall panels connected by half-grouted sleeve.

However, various types of grouting defects can arise from debris entering the construction site, inadequate air ventilation and worker errors during operations, as shown in Figure 2. These defects can substantially impair the mechanical properties of the half-grouted sleeve, thereby compromising the overall structural stability. In recent years, the incidence of fires has been increasing due to urbanization and the rise in prefabricated construction density. Consequently, there is an urgent need to investigate the performance of half-grouted sleeves with grouting defects after a fire, a topic that has garnered scholarly attention.

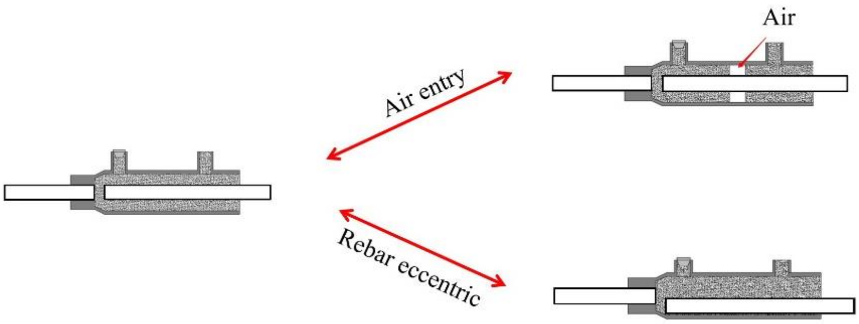

Figure 2. Defect types.

The half-grouted sleeve connection is a simple and versatile method with excellent mechanical properties for effective force transmission. Compared to cast-in-place reinforced concrete columns, precast reinforced concrete composite columns connected by half-grouted sleeves exhibit superior performance [4]. The grouted sleeve is capable of resisting the shear deformation of prefabricated columns, thus ensuring optimal connection performance [5]. It is installed within precast members and subsequently filled with grout on-site, allowing for construction without cast-in-place concrete while maintaining the integrity of the precast structures. However, due to material and manufacturing reasons, the construction of the full grouting sleeve is very complex, and joint defects are prone to occur in the construction process. Insufficient filling of sleeve grouting is one of the common typical defects in these connections, which will seriously affect the mechanical properties of joints, such as grout leakage, eccentricity of reinforcement, incomplete filling of grouting and peeling of grouting from connecting members [6]. In addition, fire is one of the most important hazards in prefabricated buildings and may occur during their service life. For prefabricated buildings in earthquake zones, not only should they meet fire-resistance requirements, but also consider seismic resistance requirements after a fire occurs. Otherwise, the building must be repaired or demolished for reconstruction after a fire occurs [7]. Compared with steel bars, cement-based grouting materials are more sensitive to high temperature. High temperature will cause complex physical and chemical changes in cement-based materials, which will reduce the bonding performance of grouting casing [8].

The use of half-grouted sleeves has become more widespread in the construction of prefabricated buildings due to their convenience. Consequently, numerous scholars have shown a strong interest in studying the properties of half-grouted sleeves under normal temperature conditions. When considering the factors involved in sleeve construction, particularly in the case of a defect-free half-grouted sleeve specimen. The primary factors that significantly affect its properties include:

(1) Sleeve factors: the material from which the sleeve is made can significantly impact its properties. Different materials have varying strength, durability, and resistance to corrosion, which can affect the overall structural integrity of the sleeve. The structural design of the sleeve, including its shape and configuration, can affect its load-bearing capacity and resistance to deformation. The reduction of inner rib spacing can improve the bearing capacity of the sleeve up to a certain extent. However, there is a limit beyond which further reduction in spacing may not provide significant benefits. The thickness of the sleeve walls can influence its strength and stiffness. Thicker sleeves generally have higher load-bearing capacity. The sleeve inner diameter of the sleeve determines the size and type of rebars that can be accommodated. It can also affect the flow and compaction of grout within the sleeve [9].

(2) Rebar factors: the diameter of the rebars used in the half-grouted sleeve can impact its dynamic loading performance and ductility. Larger diameter bars generally enhance the ductility of the grouted sleeve [10,11]. The anchorage length of rebar embedded within the sleeve affects its bonding strength with the grout. Longer anchorage lengths generally contribute to higher ultimate bearing capacity. The displacement or offset of rebar within the sleeve can influence the properties of the half-grouted sleeve [12]. Huang et al. [10] investigated that rebar offsets up to 6 mm may have negligible effects on the sleeve's properties.

(3) Grout factors: the strength of the grout used to fill the half-grouted sleeve is an important factor for optimizing its properties. Higher grout strength contributes to increased load-bearing capacity and overall performance. The level of compaction achieved during the grouting process affects the failure mode of the grouted sleeve under loading [13]. Proper compaction helps ensure better load transfer and overall stability. The water-binder ratio in the grout is crucial, especially for large-diameter sleeve connections. Strict control of the water-binder ratio is necessary to maintain the desired strength and performance of the half-grouted sleeve [14]. These factors demonstrate the complexity of designing and optimizing the properties of half-grouted sleeves in prefabricated buildings. Studying and understanding these factors can help ensure the safe and efficient use of such construction methods.

In addition, the half-grouted sleeve can cause various grouting defects at the construction site. The construction error will produce an offset effect on two kinds of parameters of the sleeve [10]. The internal structure of the sleeve, key parameters such as diameter and material have a great impact on the material strength [15]. When making test pieces, proper compaction of the material helps to ensure better load transfer and overall stability. The water-binder ratio in grouting is very important, especially for large-diameter sleeve connection [14]. Previous studies have examined the impact of end, middle and horizontal defects on grouted sleeves at normal temperatures. The presence of defects results in a reduced rebar anchorage length, which subsequently reduces the properties of the grouted sleeve [16].

Relatively speaking, the degree of insufficient grouting defect significantly affects the failure mode and properties of the half-grouted sleeve [17]. The influence of defects varies for different types of grouting defects, with the middle defect having a more significant impact than the end defect [18]. Discrete defects have lower bearing capacity than concentrated defects, and the performance of the half-grouted sleeve deteriorates as the quantity and thickness of defects increase [19]. Xie et al. [20] investigated a half-grouted sleeve connector capable of detecting and repairing defects. The mechanical properties of the repaired half-grouted sleeve were found to be essentially consistent with those of the defect-free specimen. The research under normal temperature has demonstrated that the diversity of influencing factors and the presence of defects weaken the properties of the half-grouted sleeve. This study lays a foundation for research at high temperatures.

Fire damage to buildings poses a serious threat to human life safety, making it imperative to enhance the fire resistance of prefabricated components. Previous studies have investigated the performance of grouted sleeve connectors under varying temperatures. Firstly, temperature noticeably affects the strength of grout. As the duration of exposure to high temperatures increases, the compressive and flexural tensile strength of grout diminishes [21]. Secondly, when considering half-grouted sleeves without grouting defects, the bearing capacity of the test specimens decreases with rising temperatures. Moreover, rebar bond length sufficient at normal temperature or low temperature may not be sufficient at high temperature [22]. Considering the influence of taking into account the effects of anchorage length and cooling methods, Zhu et al. [23] found that an anchoring length of 110 mm is optimal at temperatures below 400 °C. However, at temperatures of 400 °C and above, increasing the anchorage length effectively improves the ultimate bearing capacity of half-grouted sleeves. Another study by Zhang et al. [24] demonstrated that the tensile properties of half-grouted sleeve connections are significantly affected by the cooling method after a fire. Natural cooling is sufficient for maintaining the bond length, whereas water cooling falls short. The loading mode greatly influences the yield strain of the specimen when full-grouted sleeves are subjected to different loading mechanisms after high temperature. A temperature of 400 °C marks the point at which the full-grouted sleeve failure mode transitions under cyclic load. At 600 °C, none of the specimens can withstand cyclic loading [25–27]. However, there are few studies on the steering temperature of half-grouted sleeve failure mode after high temperature. In practical applications, grouted sleeves are typically encased in concrete. Consequently, Zhang et al. [28] revealed that the mechanical properties of half-grouted sleeve specimens with a concrete protective layer are less affected by high temperatures compared to those without a protective layer.

However, current research primarily focuses on the properties of fully grouted half-sleeves at high temperatures. Insufficient research has been conducted on the mechanical properties of half-grouted sleeve connectors with grouting defects after exposure to high temperatures. Furthermore, the critical temperature that significantly affects the properties of half-grouted sleeve connectors remains unestablished in existing studies. Therefore, it is necessary to study the effects of defects and temperature on the properties of half-grouted sleeves connectors.

In order to further understand the safety and reliability of half-grouted sleeve connectors with grouting defects after fire, 144 half-grouted sleeve connectors were tested under simulated high temperature fire on the basis of considering the effects of temperature and defect types. The specimens were heated at high temperature and cooled naturally. The uniaxial tensile test was carried out on the cooled specimens to observe the failure mode of the half-grouted sleeve after the test. The load-displacement curve, safety coefficient, ductility coefficient and grey correlation degree of the half-grouted sleeve specimens with grouting defects at different temperatures were analyzed and discussed, and the bond stress slip constitutive model was given, in order to study the experimental data and provide the basis for further improving the fire resistance of the connection joints of prefabricated components, so as to provide some relevant reference opinions for the safety of fabricated structures after high-temperature fire disaster.

2. Materials and Methods

2.1. Specimens Design

A total of 48 groups of specimens with half-grouted sleeves were designed and prepared to simulate various potential defects encountered in real engineering construction projects. Each group comprised three specimens, and the grouting defect types encompassed end defects, middle defects, eccentric defects, middle and end defects. Temperatures included 25 °C, 200 °C, 300 °C, 400 °C, 500 °C and 600 °C.

In the actual construction process, due to problems such as nonstandard operation, the sealing was not tight during grouting, the end of the sleeve was hollowed out, slurry leakage occurred on site and end defects were formed in the sleeve. During the grouting process, there were foreign materials in the sleeve, which could not discharge the slurry normally, so the air in the sleeve could not be completely eliminated. When the workers poured the slurry from the slurry outlet, the compressed gas of the grouting material could not flow normally, and then the grouting defect was formed in the middle of the sleeve. During the assembly of the sleeve test piece, the reinforcement was not placed and adjusted in place, and the reinforcement deviated from the center of the sleeve during grouting, resulting in eccentric defect of the reinforcement.

The GT14-BM group served as the control group, exhibiting no defects. The GT14-DB group represented an end defect. The presence of debris in the sleeve cavity in the GT14-ZB group easily caused defects in the middle of the grouted sleeve during grouting. The GT14-ZD group experienced a combination of the above-mentioned defects, leading to the occurrence of both middle and end defects. In the GT14-PX group, the grouted sleeves of the upper components were misaligned with the rebar from the lower components, causing a deviation of the anchorage end rebar from the center of the sleeve. d represents the diameter of the rebar.

The above-mentioned defects are replaced by foam glue, which mainly simulates the expansion deformation of reinforcement. The simulation figures are also shown in the following table. The foam glue offers benefits such as resistance to compression and deformation, making it a suitable replacement for the presence of defects. A 5 mm layer of foam glue was employed to accurately simulate the grouting defect (see Figure 3). Details of the specimens are presented in Table 1. The surface of the foam glue is labeled in Chinese, indicating that the material has high strength adhesion.

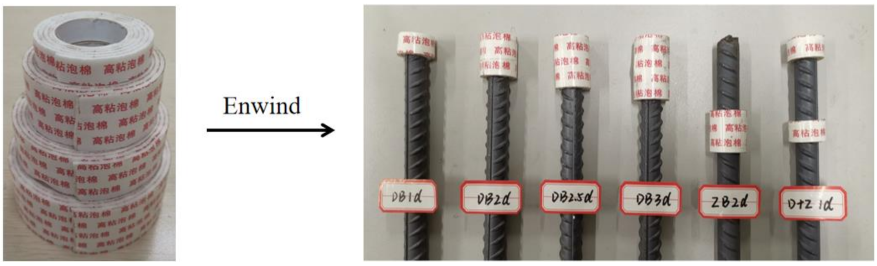

Figure 3. Defect setup.

Table 1. Details of the specimens *.

Types	Temperature/°C	Construction Defect	Defect Length	Number	Schematic Diagram
GT14-BM	25/200/300/ 400/500/600	Control group	/	18	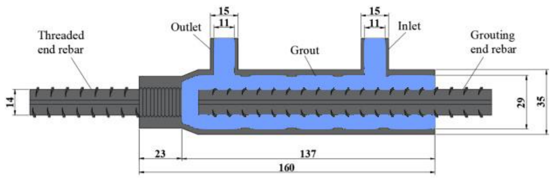

Table 1. *Cont.*

Types	Temperature/°C	Construction Defect	Defect Length	Number	Schematic Diagram
GT14-DB-1d	25/200/300/ 400/500/600	End defect	1d (14 mm)	18	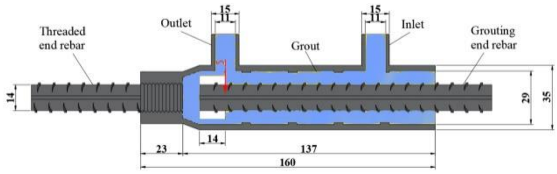
GT14-DB-2d	25/200/300/ 400/500/600	End defect	2d (28 mm)	18	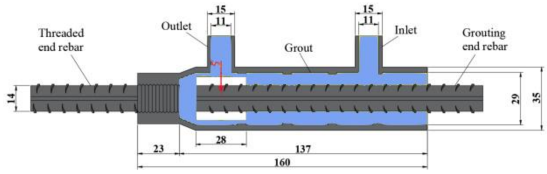
GT14-DB-2.5d	25/200/300/ 400/500/600	End defect	2.5d (35 mm)	18	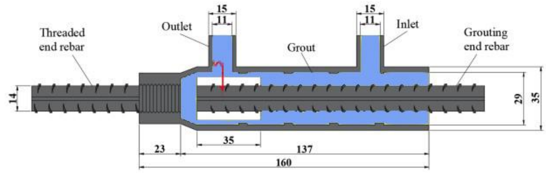
GT14-DB-3d	25/200/300/ 400/500/600	End defect	3d (42 mm)	18	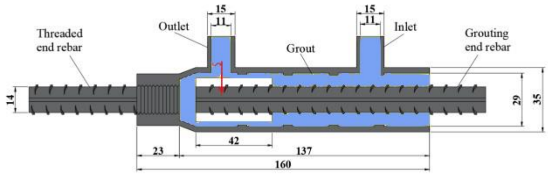
GT14-ZB-2d	25/200/300/ 400/500/600	Middle defect	2d (28 mm)	18	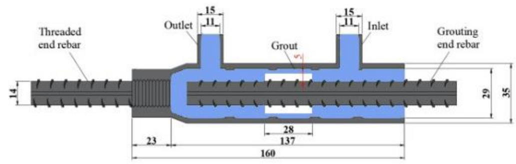
GT14-ZD-2d	25/200/300/ 400/500/600	Middle and end defect	2d (28 mm)	18	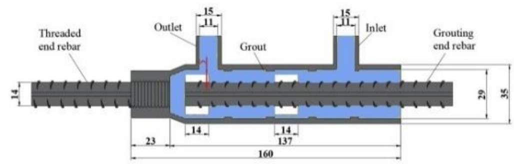
GT14-PX	25/200/300/ 400/500/600	Deviated from the center 5 mm	/	18	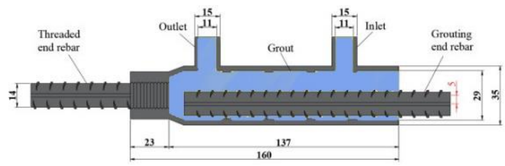

2.2. Materials

The grouted end and threaded end of the test piece are reinforced with ribbed bars with a diameter of 14 mm and a strength grade of HRB400, and the high-strength non-shrinkage grouting material produced by Shandong Haoxiang Engineering Material Technology Co., Ltd (Zibo City, China) is used in this test. The grouting material is a cement-based dry mixed material premixed with cement, fine aggregate and a variety of concrete admixtures. It has the advantages of low viscosity, good fluidity, high strength, micro expansion and non-shrinkage, and conforms to the current JG/T408-2019 [29].

A high-quality alloy steel half-grouted sleeve was employed, meeting the standards outlined in JGJ 107-2016 [30]. The profile of the sleeve is shown in Figure 4, and specific parameters are shown in Table 2.

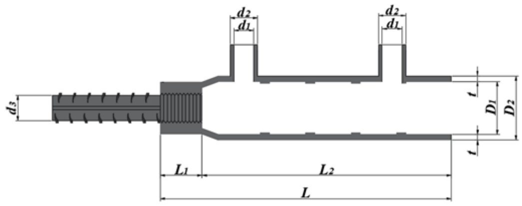

Figure 4. Axial profile of half-grouted sleeve.

Table 2. Half-grouted sleeve parameters.

Serial Number	L/mm	L_1/mm	L_2/mm	D_1/mm	D_2/mm	d_1/mm	d_2/mm	d_3/mm	t/mm
GT JB414/14	160	23	137	29	35	11	15	14	3

The threaded connection end adopts straight thread connection. By determining the length of the rebar at the threaded end, the rebar is clamped by the rebar rolling machine and thread rolling is carried out.

The grout comprises high-strength fine aggregate, cement and various additives. The fluidity test results of grout met the requirements imposed by GB/T 2419-2005 [31].

Six groups of 40 mm × 40 mm × 160 mm test blocks were made for test mechanical properties of grout according to the method of GBT 50448-2015 [32]. Each group consisted of three blocks, as seen in Figure 5. The blocks were subjected to 28 days curing period under the same conditions as the specimens. Additionally, the blocks in the high temperature group underwent heating and cooling alongside the specimens. The test results of compressive and flexural tensile strength tests on the blocks are presented in Table 3. The grout properties satisfied the minimum requirements. It can be seen that the compressive and flexural tensile strength of grout decreases as the temperature increases, indicating a significant impact of temperature on these strength properties.

(**a**) Grout properties test

Figure 5. *Cont.*

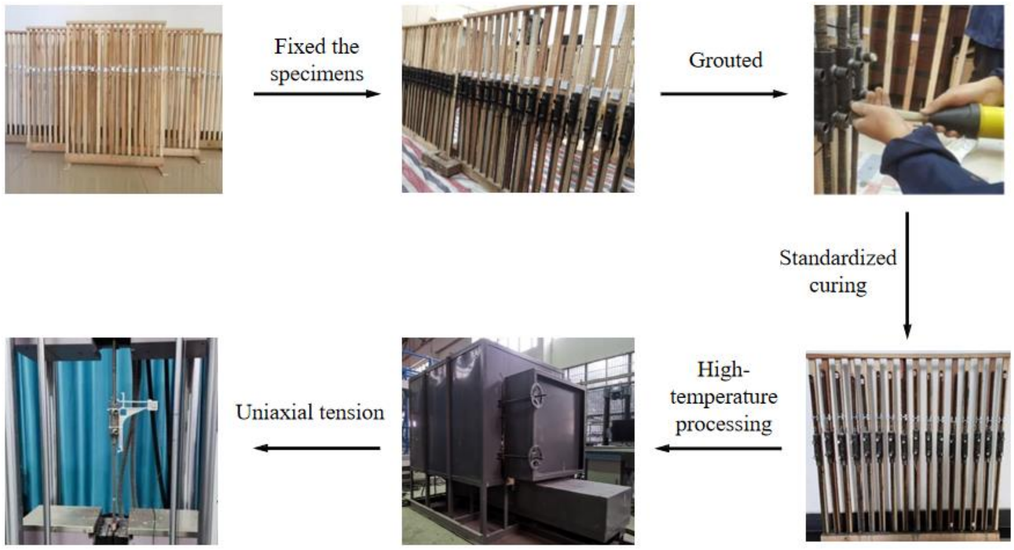

(**b**) Experimental procedure

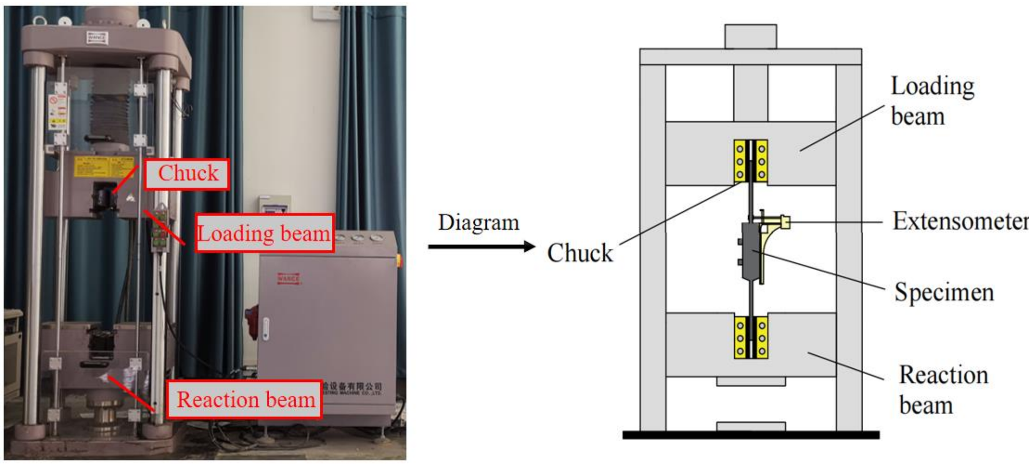

(**c**) The electronic hydraulic universal machine

Figure 5. Test step.

Table 3. Mechanical properties of grout.

Temperature/°C	Average Flexural Tensile Strength/MPa	Average Compressive Strength/MPa	Reduction Factor
25	11.75	87.3	100%
200	10.35	77.9	89.2%
300	7.34	74.4	85.8%
400	5.60	66.8	76.6%
500	4.11	63.3	72.5%
600	3.73	46.7	53.5%

The HRB400 grade rebars with a diameter of 14 mm were adopted in the specimens of both ends. Rebars subjected to high temperature were treated alongside the specimens. The test results of rebars subjected to high temperature met the minimum requirements imposed by GB/T 228.1-2021 (Table 4) [33].

Table 4. Mechanical properties of rebar at different temperatures.

Temperature/°C	Yield Strength/MPa	Tensile Strength/MPa
25	445	610
200	455	613
300	435	610
400	450	600
500	435	610
600	435	580

2.3. Fabrication Procedure

In the construction of precast concrete, first insert the rebar thread at the threaded end into the threaded end of the sleeve. Grouting holes and vent holes are connected with corrugated hoses and extend to the panel surface for subsequent grouting. Reinforcement and sleeves are then cast into precast concrete members. When the reinforcement protruding from another member is inserted into the sleeve on the upper plate, the grouting pump injects the grouting into the sleeve through the grouting hole. If grout flows out of the vent hole, stop grouting and assume that the sleeve is completely filled with grouting material. All specimens were grouted separately. The anchorage length of the grouting end is 120 mm (≥8d, not less than 8 times the diameter of the steel bar). All half-grouted sleeves are fixed to custom wood frames. The reinforcement at the grouting end shall be vertically inserted into the sleeve cavity and fixed with adhesive tape to prevent sliding. After grouting, the test piece shall be placed under standard curing conditions for 28 days. The experimental process is shown in Figure 5.

2.4. Test Setup and Loading Pattern

2.4.1. Heating Scheme

After the curing process, the specimens were heated at different high temperatures in a high-temperature electric furnace (Figure 5). The dimensions of the furnace were 1200 mm × 600 mm × 600 mm. A heating rate of 10 °C per minute was employed, and upon reaching the specified high temperature, the temperature was maintained for 2 h to ensure the specimens were uniformly heated. The heating curves for this process are depicted in Figure 5.

After the test piece reaches the constant temperature time, it shall be taken out of the furnace immediately and exposed to room temperature, allowing it to be slow and natural. During natural cooling, the test piece shall be taken out of the furnace immediately after reaching the constant temperature time and exposed to room temperature for slow natural cooling.

The time required for natural cooling at different levels of high temperature varies from 100 min to 250 min. Taking the cooling process at 600 °C as an example, it takes 250 min for the specimen to cool naturally. It is worth noting that the cooling speed can be greatly improved by using water spray cooling. Specifically, the cooling can be completed 100 min in advance by using water spray cooling at 600 °C high temperature, but there will be obvious spalling outside the sleeve, which cannot achieve the same normal specimen state as natural cooling.

After natural cooling, the specimens were subjected to a uniaxial tensile experiment.

2.4.2. Loading Scheme

The electronic hydraulic universal machine was used in this experiment, and the maximum pulling force was 600 KN (see Figure 5). The entire test and measurement were conducted using displacement control. Because most of the half-grouted sleeve specimens experienced high temperature and cooled naturally to room temperature in the test, the strength of the grouting material in the specimen is reduced and the bond slip between the reinforcement and the grouting material may fail due to the influence of high temperature. It is dangerous to control the loading rate of unidirectional tension by force, so the displacement loading method is adopted in this test. According to JGJ355-2015 [34], the loading rate was 5 mm/min, and the experiment was terminated when the specimens were damaged. An extensometer was used to measure the slip of the specimen, which was fixed on the specimens with adhesive tape. The linear deformation between the upper and lower points of the member is calculated via an extensometer and recorded as the slip value, which provides data support for the subsequent establishment of constitutive model and slip curve.

3. Results Analysis and Discussion

3.1. Failure Modes

The changes in sleeve appearance resulting from heating to specific high temperatures and subsequent cooling to normal temperature are illustrated in Figure 6. Below 200 °C, no significant alterations were observed. However, at temperatures above 300 °C, the surface of the sleeve changed from black to reddish brown, which is similar to rust, and it can be seen that some sleeves have peeling phenomena. At the intersection of grouting material and steel reinforcement, the grouting material on the side of the grouting end port peels off, and a small amount of grouting material powder adheres to the transverse ribs of the steel reinforcement. At 600 °C, the whole surface of the grouting sleeve shows a very obvious dark red. The grouting sleeve test piece was observed from the anchorage end. Under the influence of high temperature, the grouting material at the anchorage end of the sleeve reinforcement began to turn white and the surface began to develop fine lines after 400 °C high temperature. At 600 °C, the fine lines on the surface of the grouting material increase significantly.

Figure 6. Sleeve color change.

The above phenomena are analyzed from the perspective of materials science. The main reasons for its performance are as follows: the high temperature environment leads to the oxidation reaction of the material on the sleeve surface, which changes the surface color. In addition, the fire caused serious thermal stress on the surface of the sleeve, and was affected by thermal expansion, resulting in changes in the microstructure of the surface material, which led to changes in surface color and spalling.

The uniaxial tensile test of 144 half-grouted sleeve specimens showed that there were three failure modes: steel bar tensile failure, steel bar pull-out failure and steel bar sliding wire pull-out at the threaded end. The steel bar tensile failure occurred at the threaded end or grouting anchorage end, which was random. The reason for the different failure modes is that the bonding force between the grouting material and the reinforcement is greater than the ultimate strength of the reinforcement at room temperature, which shows that the reinforcement is pulled apart in the pulling process. With the increase in temperature, the bonding force decreases, and the ultimate strength of the reinforcement is greater than the bonding force, which shows that the reinforcement is pulled out. As shown in Figure 7, the tensile failure of the reinforcement occurs randomly at the threaded end and the anchorage end, and the reinforcement at the tensile failure has an obvious necking phenomenon.

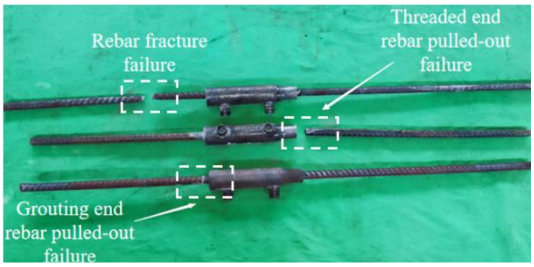

Figure 7. Failure modes.

At room temperature, the failure mode of the half-grouted sleeve specimen in the test is the tensile failure of the reinforcement and the pull-out failure of the reinforcement. The control group specimens are all the tensile failure of the reinforcement, and there is obvious necking at the tensile failure of the reinforcement. The location of tensile failure randomly appears in the threaded section or the anchorage end of the reinforcement, which has no specific rule, and may be caused by the stress concentration caused by the thread of the reinforcement. There is little difference between the failure modes in the temperature range of 200 °C~300 °C, and the control group has the phenomenon of steel bar tensile failure and steel bar pull-out failure. However, most of them are tensile failure of steel bars, which shows that there is obvious necking at the fracture of steel bars, while the control group of test pieces with pull-out failure of steel bars may be caused by the non-compaction of grouting materials during the grouting process. After 400 °C high temperature, the proportion of reinforcement pull-out failure increased, and the control group specimens with full grouting and the specimens with eccentric defects of reinforcement all appeared with the reinforcement pull-out failure mode. At the intersection of grouting material and reinforcement, the grouting material on the side of grouting end port peeled off, and the transverse rib of reinforcement was stained with a small amount of grouting material powder, which was due to the slippage between the segment sleeve and the connecting reinforcement. After the high temperature of 500 °C, the failure mode of the specimens is mostly the steel scraper pull-out failure, in which the control group with full grouting develops steel bar pull-out failure and steel bar tensile failure. The other defective specimens were all pulled out of the reinforcement. The failure phenomenon of the steel bar pull-out test piece is mostly manifested in that the grouting material at the grouting end side is separated from the sleeve wall, and it is broken as soon as it is touched, and there are more powdery grouting materials attached to the transverse rib of the pulled-out steel bar.

In the control group, which consisted of half-grouted sleeves without grouting defects, a change in failure mode from rebar fracture to rebar pulled-out failure was observed when the peak temperature reached 600 °C. Observe that the grouting material at the grouting end side has obvious fine cracks, and most of the grouting materials of the test pieces are broken into rings around the reinforcement. While pulling out the reinforcement, the massive grouting material is broken and brought out, and will be broken when touched. There is white powder grouting material on the transverse rib of the pulled-out reinforcement, and obvious grooves appear on the inner surface of the grouting end side, which is caused by the gradual pulling out of the reinforcement in the sleeve grouting section during the necking stage. At the same time, when the anchor bar in the grouting section is pulled out, brittle failure will not occur, and there is still a certain bond force between the sleeve and the reinforcement, and the bond force will gradually dissipate in the process of being pulled out. This indicated that 600 °C was the limit state of a reliable half-grouted sleeve joint. For specimens in the GT14-1/2d group, 400 °C was the transition temperatures of failure mode (see Figure 8). The limit peak temperature of specimens in GT14-DB-2.5d, GT14-DB-3d, GT14-ZD-2d and GT14-ZB-2d groups was 25 °C. At 500 °C, the failure mode for GT14-PX specimens changed from rebar fracture failure to rebar pulled-out failure. The reason for this transition is that under high temperature, the steel bars and grouting materials expand. After cooling to room temperature, the steel bars shrink, resulting in a decrease in their adsorption and friction forces with the grouting material. In addition, the compressive performance of the grouting material after cooling is affected. During the tensile process, the bonding surface between the steel bars and grouting materials is damaged by the transverse ribs of the steel bars, and the bonding strength is reduced to a certain extent, leading to a decrease in the ductility of the specimen. Deviation of 5 mm from the sleeve center had minimal influence on the half-grouted sleeves. This meant that the reliability of the half-grouted sleeve specimen was closely related to the grouting defect length, defect location and peak temperature.

(**a**) GT14-ZD-2d-300 (**b**) GT14-BM-500

Figure 8. Destruction diagram.

3.2. Bearing Capacity Analysis

In order to avoid bond failure and ensure the reliability of the connection, the bond strength of the half-grouted sleeve should be greater than the ultimate strength of the reinforcement. When the reinforcement is pulled out, the specimen is not reliable. With the increase in temperature, the ultimate load and displacement of the full group specimens are gradually reduced, and the connection performance of the specimens is gradually reduced. When the temperature exceeds 500 °C, the safety performance of the full specimen is significantly affected. When the temperature reaches 400 °C, all specimens with grouting defects are unreliable. The critical temperature of the half-grouting sleeve with grouting defects is 400 °C. Under the action of high temperature, the reinforcement and grouting material expand. After cooling to room temperature, the reinforcement retracts, which reduces the friction resistance and cementation force between the reinforcement and the slurry, and the performance of the grouting material decreases. During the tensile process, the bonding surface between the reinforcement and the grouting material is damaged by the transverse rib of the reinforcement, which reduces its stiffness. For the same type of end defects, with the increase of temperature and defect length, the yield of the specimen is more obvious, and the ultimate load decreases gradually. The larger the defect length, the smaller the total displacement, and the lower the ductility of the specimen.

The load-displacement curves were obtained via a uniaxial tensile test, as shown in Figure 9. The load was tension, and the displacement is monitored via a universal testing machine. All specimens were observed in the elastic deformation stage at the initial loading stage. These curves consist of four stages of elastic, yielding, strengthening and tightening, which looked similar to the curve of rebars under uniaxial tension. The ultimate load and yield load are shown in Table 5. The test results of three specimens in each group exhibited exceptional proximity. Therefore, the average value was utilized for analysis [35,36].

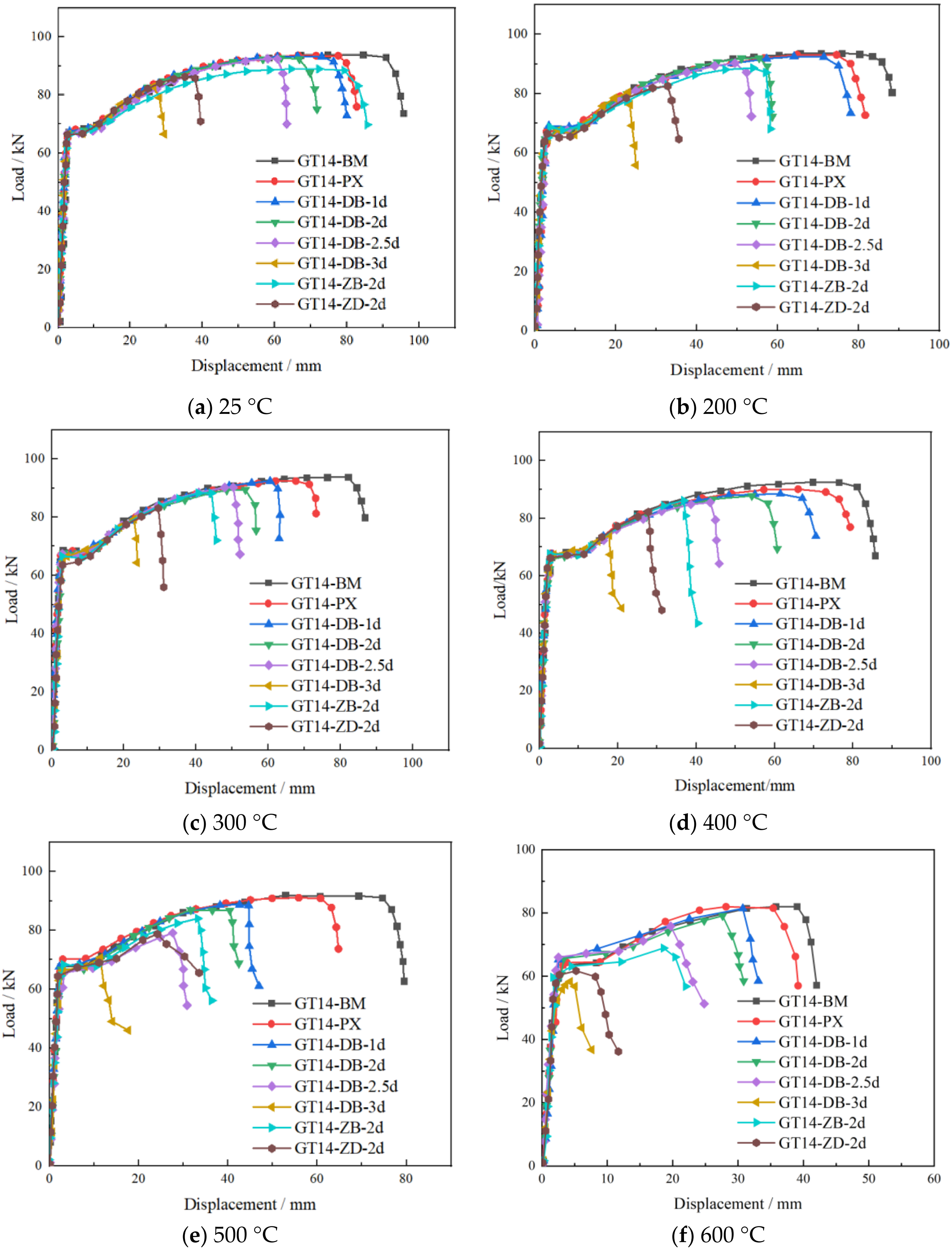

(**a**) 25 °C (**b**) 200 °C

(**c**) 300 °C (**d**) 400 °C

(**e**) 500 °C (**f**) 600 °C

Figure 9. Load-displacement curves under different temperatures.

Table 5. Experimental feature point of different groups.

Number	F_y/kN	F_u/kN	σ/MPa	Δ_y/mm	Δ_u/mm	Failure Mode
GT14-BM-25	68.47	93.87	610	2.91	84.53	Rebar fracture
GT14-BM-200	67.6	93.7	609	3.12	75.85	Rebar fracture
GT14-BM-300	68.4	93.67	608	3.17	82.14	Rebar fracture
GT14-BM-400	67.9	92.5	601	3.09	76.37	Rebar fracture
GT14-BM-500	67.2	92.02	598	2.56	69.27	Rebar fracture
GT14-BM-600	63.48	81.9	532	3.25	35.83	Rebar pulled-out
GT14-DB-1d-25	67.5	93.3	605	3.19	73.09	Rebar fracture
GT14-DB-1d-200	68.8	92.75	601	3.52	71.42	Rebar fracture
GT14-DB-1d-300	67.07	92.37	600	2.54	60.55	Rebar fracture
GT14-DB-1d-400	67.5	88.26	573	3.21	61.5	Rebar pulled-out
GT14-DB-1d-500	67.64	88.45	575	2.24	42.62	Rebar pulled-out
GT14-DB-1d-600	65.23	81.34	528	2.53	30.74	Rebar pulled-out
GT14-DB-2d-25	67.89	92.3	600	3.09	61.78	Rebar fracture
GT14-DB-2d-200	67.75	92.07	598	2.67	55.43	Rebar fracture
GT14-DB-2d-300	67.2	89.21	580	3.38	53.67	Rebar fracture
GT14-DB-2d-400	66.69	87.86	571	3.09	54.2	Rebar pulled-out
GT14-DB-2d-500	66.7	86.3	561	2.72	40.43	Rebar pulled-out
GT14-DB-2d-600	65.6	79.08	514	3.38	27.64	Rebar pulled-out
GT14-DB-2.5d-25	66.84	92.4	600	2.54	60.8	Rebar pulled-out
GT14-DB-2.5d-200	67.2	90.33	587	3.21	49.45	Rebar pulled-out
GT14-DB-2.5d-300	66.9	90.2	586	2.92	50.34	Rebar pulled-out
GT14-DB-2.5d-400	66.5	85.46	555	2.97	43.6	Rebar pulled-out
GT14-DB-2.5d-500	66.6	79.08	514	3.38	27.64	Rebar pulled-out
GT14-DB-2.5d-600	66.2	75.77	492	2.54	19.71	Rebar pulled-out
GT14-DB-3d-25	66.5	82.86	538	2.87	26.44	Rebar pulled-out
GT14-DB-3d-200	64.53	80.56	523	3.29	23.13	Rebar pulled-out
GT14-DB-3d-300	64	79.3	515	3.21	22.8	Rebar pulled-out
GT14-DB-3d-400	67.34	74.1	481	3.62	17.84	Rebar pulled-out
GT14-DB-3d-500	66.3	70.64	459	3.02	11.45	Rebar pulled-out
GT14-DB-3d-600	/	58.29	379	2.33	4.29	Rebar pulled-out
GT14-ZB-2d-25	67.14	88.9	578	3.29	72.34	Rebar pulled-out
GT14-ZB-2d-200	67.24	88.67	576	3.79	53.95	Rebar pulled-out
GT14-ZB-2d-300	66.4	88.26	573	2.91	40.7	Rebar pulled-out
GT14-ZB-2d-400	67.8	84	546	2.72	36.85	Rebar pulled-out
GT14-ZB-2d-500	67.18	82.19	534	3.22	33.23	Rebar pulled-out
GT14-ZB-2d-600	63.15	68.87	447	1.70	18.61	Rebar pulled-out
GT14-ZD-2d-25	66.4	86.23	560	2.64	35.12	Rebar pulled-out
GT14-ZD-2d-200	66.2	82.59	537	3.11	32.86	Rebar pulled-out
GT14-ZD-2d-300	63.61	83.09	540	3.08	29.56	Rebar pulled-out
GT14-ZD-2d-400	66.19	82.16	534	2.81	27.79	Rebar pulled-out
GT14-ZD-2d-500	64.39	78.76	512	1.95	24.22	Rebar pulled-out
GT14-ZD-2d-600	/	60.4	392	2.68	5.24	Rebar pulled-out
GT14-PX-25	68.16	93.6	608	2.64	77.65	Rebar fracture
GT14-PX-200	67.5	93.1	605	2.91	74.57	Rebar fracture
GT14-PX-300	67.63	92.37	600	2.54	67.67	Rebar fracture
GT14-PX-400	67.79	90.1	585	3.09	66.02	Rebar fracture
GT14-PX-500	69.92	90.08	585	3.01	55.90	Rebar pulled-out
GT14-PX-600	64.3	81.4	529	3.25	28.17	Rebar pulled-out

The influence of temperature and defects on the mechanical properties of half-grouted sleeves was analyzed using safety factor, ductility factor and grey correlation. The experimental data for different defect groups are presented in Table 5. The data were obtained through uniaxial tensile testing. F_y represents the yield load, which is the load when the half-grouted sleeve begins to yield. Fu represents the ultimate load, which is the maximum load the half-grouted sleeve can bear during the stretching process. σ represents the stress of the rebar, calculated using $\sigma = \frac{F_u}{\pi r^2}$, where r is the radius of the rebar. Δ_y represents the yield elongation, which is the corresponding displacement value when the half-grouted sleeve specimen starts to yield. Δ_u represents the ultimate elongation, which is the displacement value corresponding to the ultimate load. The ultimate tensile force and yield tensile force of each group showed a decreasing trend with increasing temperature and defect length. However, the yield load remained relatively stable. At 600 °C, the ultimate load of GT14-DB-2d decreased by 14.3%. Among them, the yield load changed little. When the rebar fracture occurred, the rebar stress in the half-grouted sleeve specimen was similar to that of a single rebar. The stress in the GT14-DB-1d specimen at 400 °C was 95% of that in a single rebar. The ultimate tensile force and yield tensile force of the half-grouted sleeve were consistently lower than those of a single rebar when the failure mode was rebar pulled-out. The yield elongation increased with temperature, while the ultimate elongation of defective specimens at different temperatures was smaller than that of the control group. The ultimate elongation of the half-grouted sleeve specimens with a change in failure mode increased with temperature when the failure mode was rebar fracture but decreased when the failure mode was bonding failure. These results demonstrate that temperature, defect length and type significantly affect the yield elongation and ultimate elongation.

Taking the loading of the test piece as the evaluation standard, the safety factor is artificially specified here, which is recorded as α. The safety factor is determined by the ratio of ultimate load to yield load. The formula is as follows:

$$\alpha = \frac{P_u}{P_y} \tag{1}$$

α is expressed as safety factor in the formula, P_u is the ultimate load and P_y is the yield load.

From the formula, the safety factors of each group of specimens between 0.8 and 1.4 are calculated. When the safety factor is higher, the safety of the specimen can be guaranteed; that is, the negative impact of defects on the structure at high temperature is smaller. The linear change in safety factor of each group of test pieces in the environment from low temperature to high temperature is shown in the following figure.

When the temperature reaches 400 °C, all the defective specimens with reduced anchorage length will fail. Different types of defects have different effects on the mechanical properties of half-grouted sleeve specimens. Among them, the 3d defect at the end has the greatest impact on the tensile properties of the grouting sleeve connection, and the decline rate of the safety factor is relatively mild between 25 °C and 400 °C, but it drops sharply with the loading after 400 °C. For the fully grouted specimen with temperature higher than 500 °C, the original reliable half-grouted sleeve specimen becomes unreliable. Although high temperature and grouting defects have an important impact on the reliability of half-grouted sleeve connectors, defects are more likely to have adverse effects than high temperature under the extreme environment of the same temperature, especially 600 °C.

The safety factor α of the half-grouted sleeve after high temperatures can be calculated via Equation (1). F_u represents the ultimate load of each group of specimens. F_y (25) represents the yield load of GT14-BM group at 25 °C. F_u and $F_y(25)$ can be obtained from Table 6.

$$\alpha = \frac{F_u}{F_y(25)} \tag{2}$$

Taking the deformation of the specimen during loading as the evaluation standard, the ductility coefficient is artificially specified here, which is recorded as β. The safety factor is determined by the ratio of limit displacement to yield displacement. The formula is as follows:

$$\beta = \frac{\mathrm{D_u}}{\mathrm{D_y}} \tag{3}$$

β is the ductility coefficient in the formula, $\mathrm{D_u}$ is the ultimate displacement and $\mathrm{D_y}$ is the yield displacement.

Table 6. Grey correlation data.

Number	Defect Types X_1	Temperature X_2/°C	Ultimate Load X_0/kN	$\overline{X_1}$	$\overline{X_2}$	$\overline{X_0}$	Δ_1	Δ_2	ξ_1	ξ_2
1	GT14-BM	200	93.7	1	1	1	0	0	1	1.00
2	GT14-BM	300	93.67	1	1.5	1	0	0.50	1	0.70
3	GT14-BM	400	92.5	1	2	0.99	0.01	1.01	0.99	0.54
4	GT14-BM	500	92.02	1	2.5	0.98	0.02	1.52	0.99	0.44
5	GT14-BM	600	81.9	1	3	0.87	0.13	2.13	0.90	0.36
6	GT14-DB-1d	200	92.75	0.88	1	0.99	0.11	0.01	0.92	0.99
7	GT14-DB-1d	300	92.37	0.88	1.5	0.99	0.10	0.51	0.92	0.70
8	GT14-DB-1d	400	88.26	0.88	2	0.94	0.06	1.06	0.95	0.53
9	GT14-DB-1d	500	88.45	0.88	2.5	0.94	0.06	1.56	0.95	0.43
10	GT14-DB-1d	600	81.34	0.88	3	0.87	0.02	2.13	0.99	0.36
11	GT14-DB-2d	200	92.07	0.77	1	0.98	0.22	0.02	0.85	0.99
12	GT14-DB-2d	300	89.21	0.77	1.5	0.95	0.19	0.55	0.87	0.68
13	GT14-DB-2d	400	87.86	0.77	2	0.94	0.17	1.06	0.87	0.53
14	GT14-DB-2d	500	86.3	0.77	2.5	0.92	0.15	1.58	0.89	0.43
15	GT14-DB-2d	600	79.08	0.77	3	0.84	0.08	2.16	0.94	0.36
16	GT14-DB-2.5d	200	90.33	0.71	1	0.96	0.26	0.04	0.82	0.97
17	GT14-DB-2.5d	300	90.2	0.71	1.5	0.96	0.25	0.54	0.82	0.69
18	GT14-DB-2.5d	400	85.46	0.71	2	0.91	0.20	1.09	0.85	0.52
19	GT14-DB-2.5d	500	79.08	0.71	2.5	0.84	0.14	1.66	0.90	0.42
20	GT14-DB-2.5d	600	75.77	0.71	3	0.81	0.10	2.19	0.92	0.35
21	GT14-DB-3d	200	80.56	0.65	1	0.86	0.21	0.14	0.85	0.89
22	GT14-DB-3d	300	79.3	0.65	1.5	0.85	0.20	0.65	0.86	0.65
23	GT14-DB-3d	400	74.1	0.65	2	0.79	0.14	1.21	0.89	0.50
24	GT14-DB-3d	500	70.64	0.65	2.5	0.75	0.10	1.75	0.92	0.41
25	GT14-DB-3d	600	58.29	0.65	3	0.62	0.03	2.38	0.98	0.33
26	GT14-ZB-2d	200	88.67	0.77	1	0.95	0.18	0.05	0.87	0.96
27	GT14-ZB-2d	300	88.26	0.77	1.5	0.94	0.18	0.56	0.87	0.68
28	GT14-ZB-2d	400	84	0.77	2	0.90	0.13	1.10	0.90	0.52
29	GT14-ZB-2d	500	82.19	0.77	2.5	0.88	0.11	1.62	0.92	0.42
30	GT14-ZB-2d	600	68.87	0.77	3	0.74	0.03	2.26	0.97	0.34
31	GT14-ZD-2d	200	82.59	0.77	1	0.88	0.11	0.12	0.91	0.91
32	GT14-ZD-2d	300	83.09	0.77	1.5	0.89	0.12	0.61	0.91	0.66
33	GT14-ZD-2d	400	82.16	0.77	2	0.88	0.11	1.12	0.92	0.53
34	GT14-ZD-2d	500	78.76	0.77	2.5	0.84	0.07	1.66	0.94	0.45
35	GT14-ZD-2d	600	60.4	0.77	3	0.64	0.12	2.36	0.91	0.34
36	GT14-PX	200	93.1	1	1	0.99	0.01	0.01	0.99	0.99
37	GT14-PX	300	92.37	1	1.5	0.99	0.01	0.51	0.99	0.70
38	GT14-PX	400	90.1	1	2	0.96	0.04	1.04	0.97	0.53
39	GT14-PX	500	90.08	1	2.5	0.96	0.04	1.54	0.97	0.44
40	GT14-PX	600	81.4	1	3	0.87	0.13	2.13	0.90	0.36

When the temperature reaches 400 °C, all the defective specimens with reduced anchorage length will fail. The high temperature has a great influence on the flexural and compressive properties of the grouting material. At 600 °C, the flexural strength of the grouting material decreases by 68%, and the compressive strength decreases by 46.5%. The high temperature has little effect on the mechanical properties of the reinforcement, and the reinforcement still has sufficient strength at 600 °C.

From the deformation point of view, when the temperature reaches 400 °C, for the end defect specimen, when the defect length is less than or equal to 2D, the failure mode of the half-grouted sleeve specimen changes. When the defect length is greater than 2D, the specimen is unreliable at room temperature. The reason is as follows: the compressive strength of the grouting material decreases due to high temperature. With the increase of temperature, the longer the defect length, the shorter the effective anchorage length of the reinforcement, the less the bonding force between the reinforcement and the grouting material, the lower its bearing capacity, and the half-grouted sleeve specimen is more prone to failure.

The ductility factor β of the half-grouted sleeve after high temperatures can be calculated via Equation (2). Δu indicates the ultimate elongation of each group. Δy (25) represents the yield elongation of GT14-BM group at 25 °C. Δu and Δy (25) can be obtained from Table 6.

$$\beta = \frac{\Delta_u}{\Delta_y(25)} \tag{4}$$

The stress depends on the bearing capacity of the weld between the reinforcement and the grouting sleeve and the bonding force of the reinforcement materials around the weld. Therefore, it is necessary to strengthen and improve the anti-high temperature damage of grouting sleeve components. For example, for the test results at high temperature, compared with the FRP bare reinforcement, BFRP reinforcement can be used as one of the components of the test component. Chopped basalt fiber reinforced cement can be selected as the cladding layer to provide better oxygen isolation for BFRP bars. The residual mechanical properties of BFRP bars with cladding layer are generally high at high temperature, and the percentage of residual elastic modulus of BFRP bars is still more than 70% at 400 °C, the thickness of the clamping layer is 70 mm, the coating layer doped with chopped basalt fiber has excellent high temperature resistance and anti-cracking performance [37]. By comparing the ultimate strength of the half-grouted sleeve with different thicknesses of protective layer at different temperatures, it can be found that the ultimate strength and displacement of the specimen with protective layer are significantly increased, indicating that an appropriate increase in the thickness of the protective layer can effectively improve the ultimate strength of the half-grouted sleeve, and the thickness of the protective layer can be appropriately increased at the connection part in the project. Quantitative data show that with the increase in anchorage length, the ultimate strength of the half-grouted sleeve does not increase significantly before 400 °C, which indicates that the reinforcement is broken. When the temperature is lower than 400, the optimal anchorage length of the sample is 110 mm [17]. When the temperature is higher than 400 °C, increasing the anchorage length can effectively improve the ultimate bearing capacity of the specimen. At 600 °C, the increase in anchorage length significantly improves the ultimate strength and ultimate displacement of the half-grouted casing, indicating that the increase in anchorage length can effectively improve the fire resistance of the connecting part.

3.2.1. Analysis at 25 °C~200 °C

The safety factor is shown in Figure 10. For the same end defect, the safety factor gradually decreases with the increase in defect length. The safety factor of the GT14-DB-3d group decreased significantly. The ductility coefficient is shown in Figure 11. Under the same end defect, the decreasing trend of the ductility coefficient is more obvious with the increase in defect length. When the defect length increases from 28 mm to 35 mm, the test piece cannot meet the construction use at room temperature. Because the defect length is too large, the anchorage length decreases, and the cementation force between the reinforcement and the grouting material is far less than the ultimate tensile strength of the reinforcement. The load-displacement curves of specimens with different defects at 25 °C are shown in Figure 11. The load and displacement of the specimen in the elastic stage have a linear relationship, and the displacement increases significantly after entering the strengthening stage. The decline rate of each curve in the failure stage is not exactly the same. At 25 °C, the specimens of GT14-BM, GT14-DB-1D, GT14-DB-2D and GT14-PX were damaged by steel bar tension, and the other specimens were damaged by steel bar pullout. The pull-out failure of reinforcement indicates that some defective specimens are unreliable at room temperature. At room temperature, the ultimate load of GT14-DB-2d and GT14-DB-3d specimens decreased by 1.7% and 11.7% compared with the full group specimens. The load displacement curves of specimens with different defects at 200 °C are shown in Figure 12. The overall failure mode of all defective specimens is roughly the same as that at 25 °C. The influence of 200 °C on the failure mode of half-grouted sleeve specimens is relatively small. The ultimate load and ultimate elongation of the specimens with defects are lower than those of the full group. At 200 °C, the ultimate load of GT14-DB-2d and GT14-DB-3d specimens was reduced by 1.7% and 14% compared to the full group specimens. 200 °C has little effect on the performance of the half-grouted sleeve, and reliable specimens at room temperature are still reliable at 200 °C. The safety coefficient and ductility coefficient are shown in the figure, and the overall trend is similar to 25 °C. At 200 °C, the defect has a greater impact on the half-grouted sleeve.

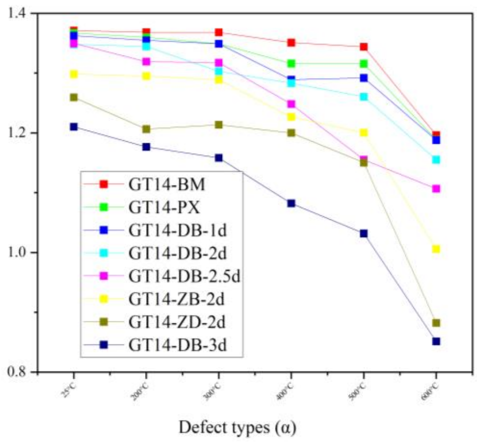

(**a**) Safe factor α

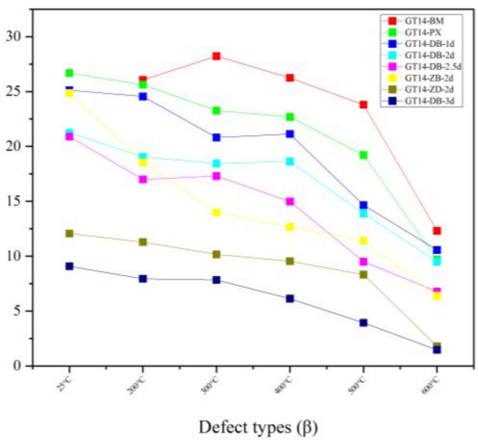

(**b**) Ductility factor β

Figure 10. α and β under different defect types.

3.2.2. Analysis at 300 °C~400 °C

The load-displacement curves of specimens with different defects at 300 °C are shown in Figure 13. At 300 °C, GT14-DB-2.5d, GT14-DB-3d, gt14-zb-2d and gt14-zd-2d specimens were pulled out. The ultimate load of GT14-DB-2.5d and gt14-zb-2d specimens at 300 °C decreased by 18% and 22.3% compared with that at room temperature. The safety factor and ductility factor are shown in the figure. At 300 °C, the safety factor of GT14-DB-3d and gt14-zd-2d groups is 15.3% and 11.7% lower than that of gt14-bm group. The ductility coefficients of GT14-DB-2d and gt14-zb-2d specimens at 300 °C were 34.7% and 50.5% lower than those of gt14-bm specimens. The influence of 300 °C on the strength of the half-grouted sleeve increases. The load-displacement curves of specimens with different defects at 400 °C are shown in Figure 13. After yielding, the rising rate of the curve is different, and it shows a different downward trend after failure. At 400 °C, the failure mode of GT14-DB-1d and GT14-DB-2d specimens changed from tensile failure to pull-out failure. The ultimate load of GT14-DB-2d group specimens at room temperature and 400 °C is 1.7% and 5% lower than that of the full group specimens. When the temperature rises to 400 °C, the ultimate load and ultimate displacement of the GT14-DB-2d specimen are less than that of GT14-DB-1d specimen. When the length of the end defect increases from 14 mm to 28 mm, the connection performance of the specimen decreases slightly. As the mechanical properties of the grouting material decrease after high temperature, the bonding force between the reinforcement and the grouting material decreases, and the specimen is more prone to pull-out failure. When the temperature reaches 400 °C, the influence of high temperature on the performance of the half-grouting sleeve is higher than that of defects.

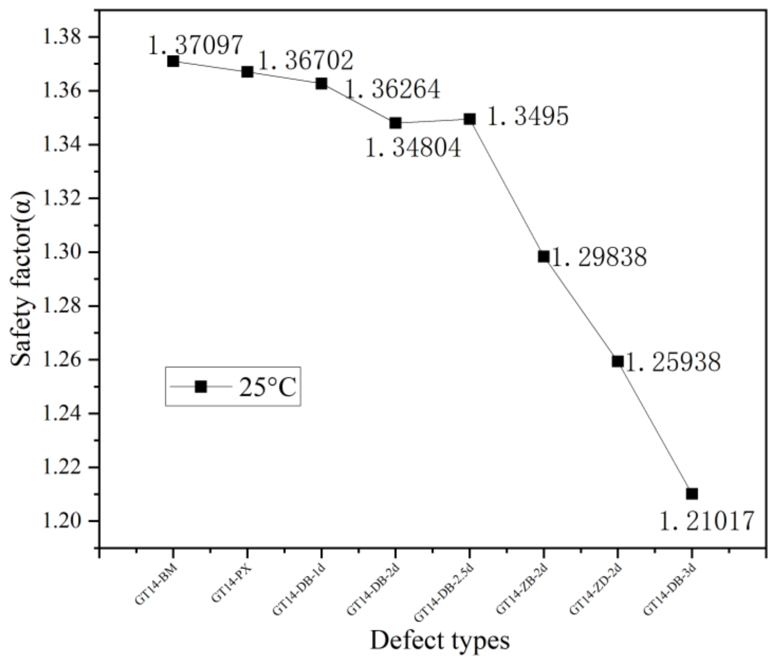

(**a**) Safe factor

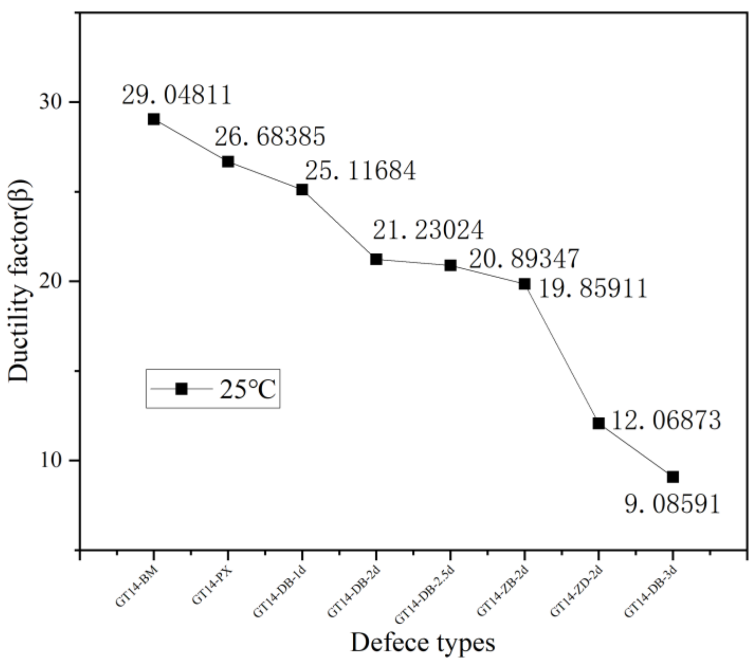

(**b**) Ductility factor

Figure 11. Safe factor and ductility factor at 25 °C.

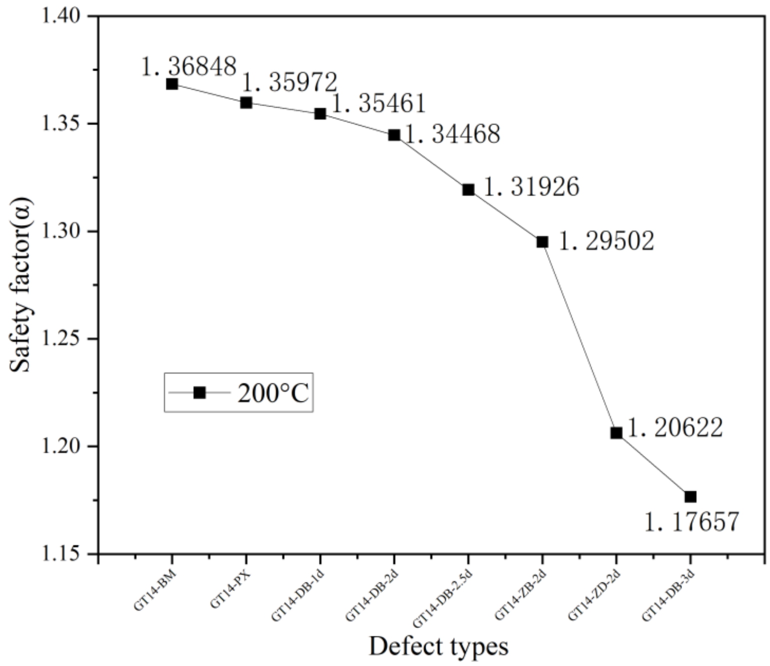

(**a**) Safe factor

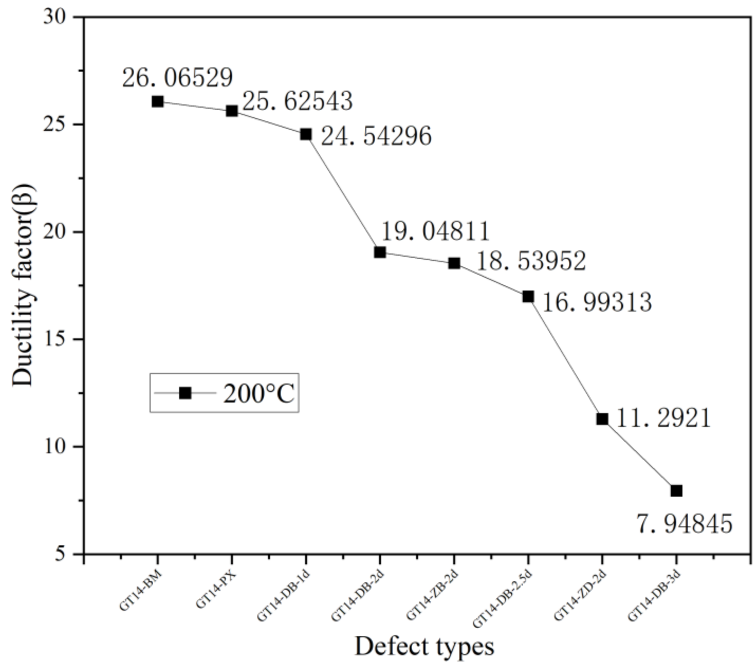

(**b**) Ductility factor

Figure 12. Safe factor and ductility factor at 200 °C.

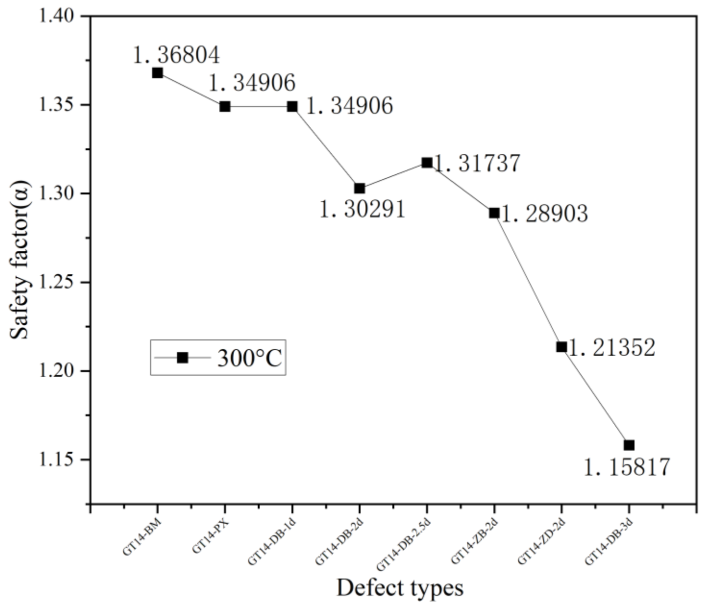

(**a**) Safe factor

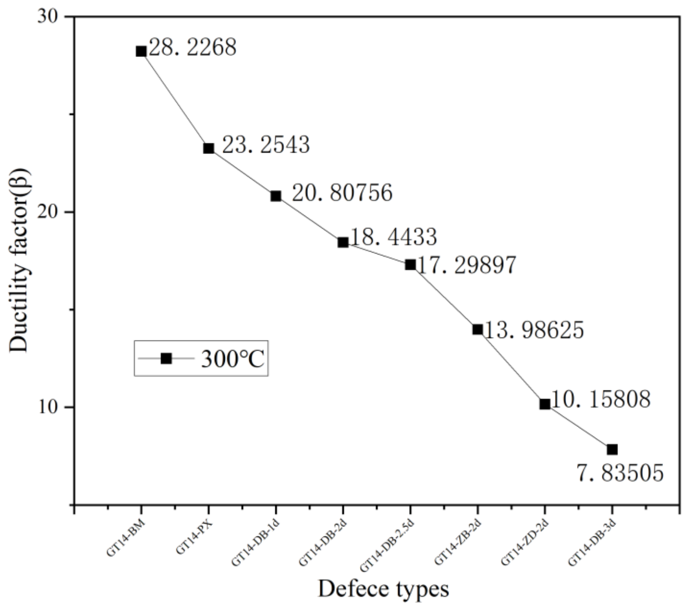

(**b**) Ductility factor

Figure 13. Safe factor and ductility factor at 300 °C.

3.2.3. Analysis at 500 °C~600 °C

The load-displacement curves of specimens with different defects at 500 °C are illustrated in Figure 14. The curves had an obvious yield stage. When the temperature reaches 500 °C, the failure mode of specimens in the GT14-PX group changed to rebar pulled-out failure. The ultimate load of GT14-ZB-2d group at 500 °C was 10.7% lower than that of GT14-BM. At 500 °C, the safety factor of the GT14-DB-3d specimen was reduced by 14.9% compared with normal temperature, and the ductility factor of the GT14-ZB-2d specimen was reduced by 54.1% compared with normal temperature, as shown in Figure 14. The effect of high temperature reduces the compressive and flexural strength of grout, leading to a decrease in the ductility of the test piece. The tensile property of deviation from the center 5 mm specimen is greatly affected when the temperature exceeds 500 °C. According to Figure 15, GT14-DB-3d and GT14-ZD-2d group curves did not exhibit a yield stage.

Subsequently, after reaching the peak load, the displacement experienced a sharp decrease, leading to a rebar pulled-out failure. At 600 °C, the failure mode of GT14-BM group was changed to rebar pulled-out failure. All the specimens were damaged by rebar pulled-out, and the bonding force between rebar and grout was less than the ultimate strength of rebar, resulting in failure of the specimens. The half-grouted sleeves that are reliable at normal temperature become unreliable at 600 °C. The safety factor and ductility factor are shown in Figure 16. At 600 °C, the ductility factor of the GT14-BM group decreased by 48% compared with that at 25 °C. The mechanical properties of half-grouted sleeve are degraded seriously at 600 °C.

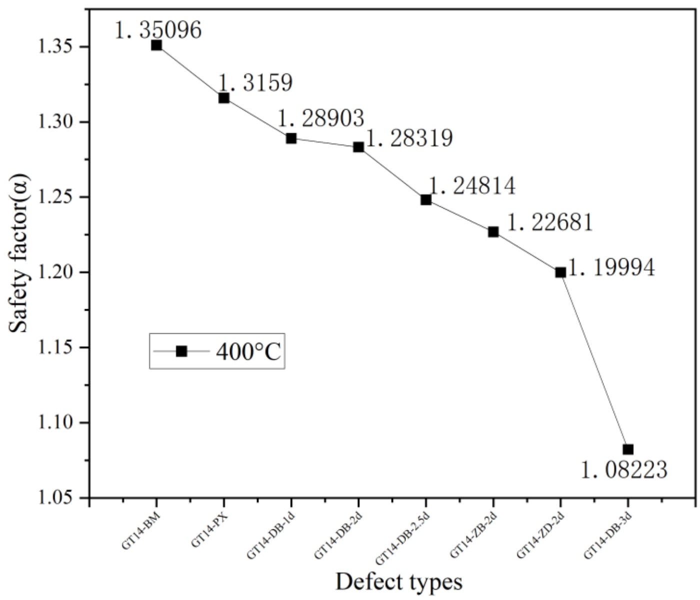

(**a**) Safe factor

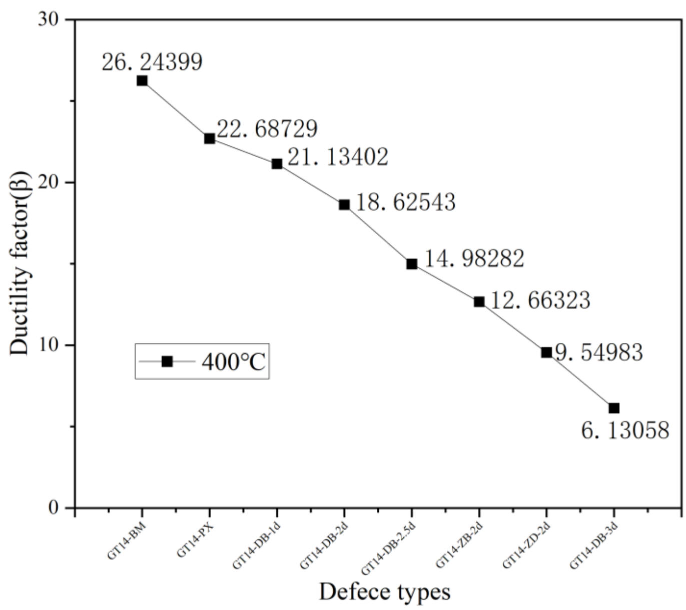

(**b**) Ductility factor

Figure 14. Safe factor and ductility factor at 400 °C.

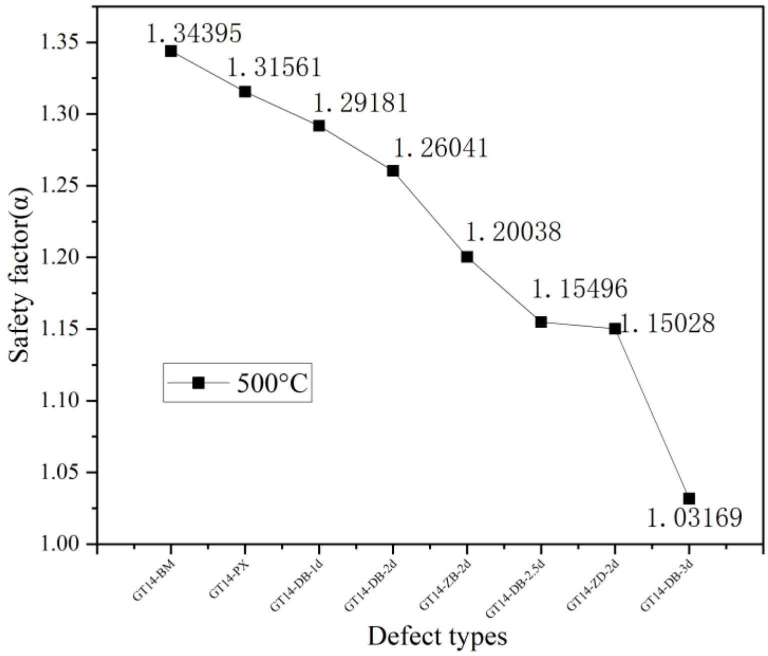

(**a**) Safe factor

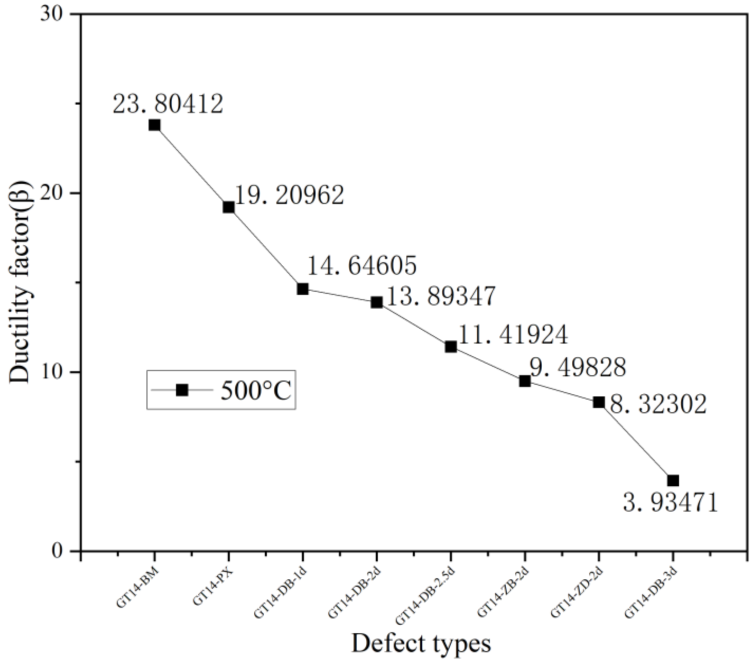

(**b**) Ductility factor

Figure 15. Safe factor and ductility factor at 500 °C.

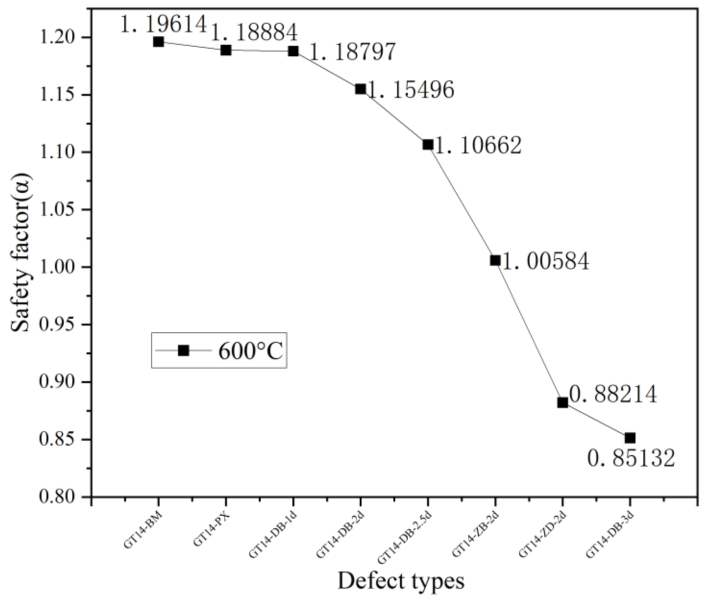

(**a**) Safe factor

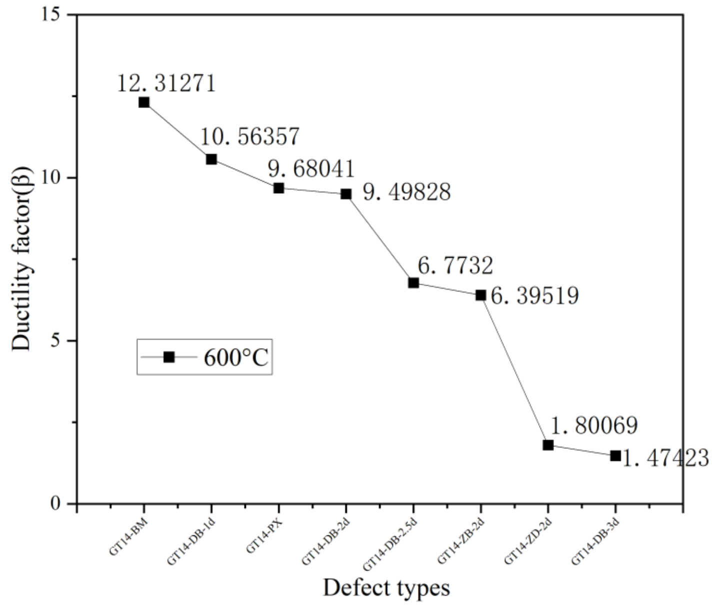

(**b**) Ductility factor

Figure 16. Safe factor and ductility factor at 600 °C.

In order to ensure the reliability of the connections and avoid bond failure, the bond strength of half-grouted sleeves should exceed the ultimate strength of the rebar. When the rebar was pulled out, the specimen was not reliable. As the temperature increased, the ultimate load and ultimate displacement of the specimens progressively decreased. The connection performance of the specimens gradually deteriorated. Exceeding 500 °C, the safety performance of the specimen is considerably compromised. All specimens with grouting defects are unreliable when the temperature reached 400 °C. The critical temperature for a half-grouted sleeve with grouting defects is 400 °C. The properties of the grout diminish when the half-grouted sleeve is subjected to heat. Both the rebar and grout undergo expansion under high temperatures. Moreover, the cementation force and frictional resistance between the rebar and grout decreased after cooling. The stiffness decreases as micro-cracks form among the rebar and grout. Comparing the same end defect type, the specimen entered the yield stage faster with the increase in temperature and defect length. The end defect shortens the effective anchorage length between the rebar and grout, and the strength of the grout decreases after heating. Consequently, as the temperature rises and the defect length increases, the bearing capacity of the specimen is significantly reduced, eventually leading to the rebar being pulled out. Therefore, the half-grouted sleeve specimen with a middle defect is more susceptible to rebar pulled-out failure compared to one with an end defect. This can be attributed to the influence of defect placement on the force transfer effect between the grout and the rebar. When defects are located farther away from the sleeve end, the bearing capacity decreases for connectors with the same total effective anchor lengths. The connectors with identical total defect lengths exhibit lower bearing capacity when possessing discrete defects compared to concentrated defects. The defects cause the grout to be divided into multiple stress sections, leading to a discontinuous transmission path that significantly impacts the bearing capacity of the specimens.

The safety factor and ductility factor of the half-grouted sleeve specimen without defect and with defect decreased with the increase in temperature. The safety factor and ductility factor of defective specimens were consistently smaller than that of the control group at different temperatures. As the defect length increased, the safety factor and ductility factor decreased. The GT14-DB-3d group exhibited the lowest safety factor and the least reliability. The properties of the half-grouted sleeve are significantly influenced by both high temperatures and defects.

3.3. Grey Correlation Analysis of Ultimate Strength

Grey correlation measures the geometric similarity between reference sequence and comparison sequence. However, the grey correlation analysis method may be influenced by subjective factors when determining the correlation degree and weight, cannot handle large and complex datasets and has weak ability to handle non-linear relationships. Compared with other analysis methods, grey correlation degree has no obvious advantages in reducing data complexity and refining main features. Due to the relevant characteristics of this experiment, grey correlation analysis can be used.

A higher similarity between reference sequence and comparison sequence indicates a stronger correlation, and vice versa. Through the analysis of the test data, the influence of different defect types and temperature on the strength of the specimen was studied. The reference sequence was set as the ultimate load, while the comparison sequence consisted of defect degree and temperature. The purpose is to compare the correlation between defect degree and temperature with regard to their impact on the strength of specimens.

Grey correlation data were selected for different construction defect types, temperature and ultimate load. Anchorage length values were also selected for different defect types, which is X1. The temperature was X2 and the ultimate load was X0. The reference sequence and comparison sequence were numerically initialized. The proximity was then calculated by subtracting the comparison sequence value from the corresponding test sequence value and taking the absolute value. This absolute value represents the sequence's value, which can get Δ1 and Δ2. The correlation coefficient can be calculated using Equation (5):

$$\xi_{\mathrm{i}}(k) = \frac{\Delta_{\mathrm{min}} + \rho\Delta_{\mathrm{max}}}{\Delta_i(k) + \rho\Delta_{\mathrm{max}}} \tag{5}$$

where ρ is the resolution coefficient, which is 0.5, Δmin is the minimum value of proximity and Δmax is the maximum value of proximity. Table 6 presents the results obtained from calculating a series of correlation coefficients.

Equation (4) was used to calculate the correlation degree:

$$\xi_{\mathrm{i}}(k) = \frac{\Delta_{\min} + \rho\Delta_{\max}}{\Delta_i(k) + \rho\Delta_{\max}} \tag{6}$$

where $\gamma_i \geq 0.6$ indicates a strong association between the comparison series and reference sequence factors, while $\gamma_i < 0.6$ indicates a poor correlation. $\gamma_i < 0.5$ signifies no correlation between the comparison sequence and the reference sequence.

The calculated correlation degree of different defect types is 0.92, which is higher than the correlation coefficient of 0.59 for temperature. The analysis shows that the two factors of different defect types and temperature are related to the ultimate load. However, the influence degree of different defects is greater than that of temperature.

3.4. Bond Stress-Slip Constitutive Model

The relationship between bonding stress and slip obtained through experiments was used to summarize the specimens with the most unfavorable performance at various temperatures. The results are shown in Figures 17 and 18.

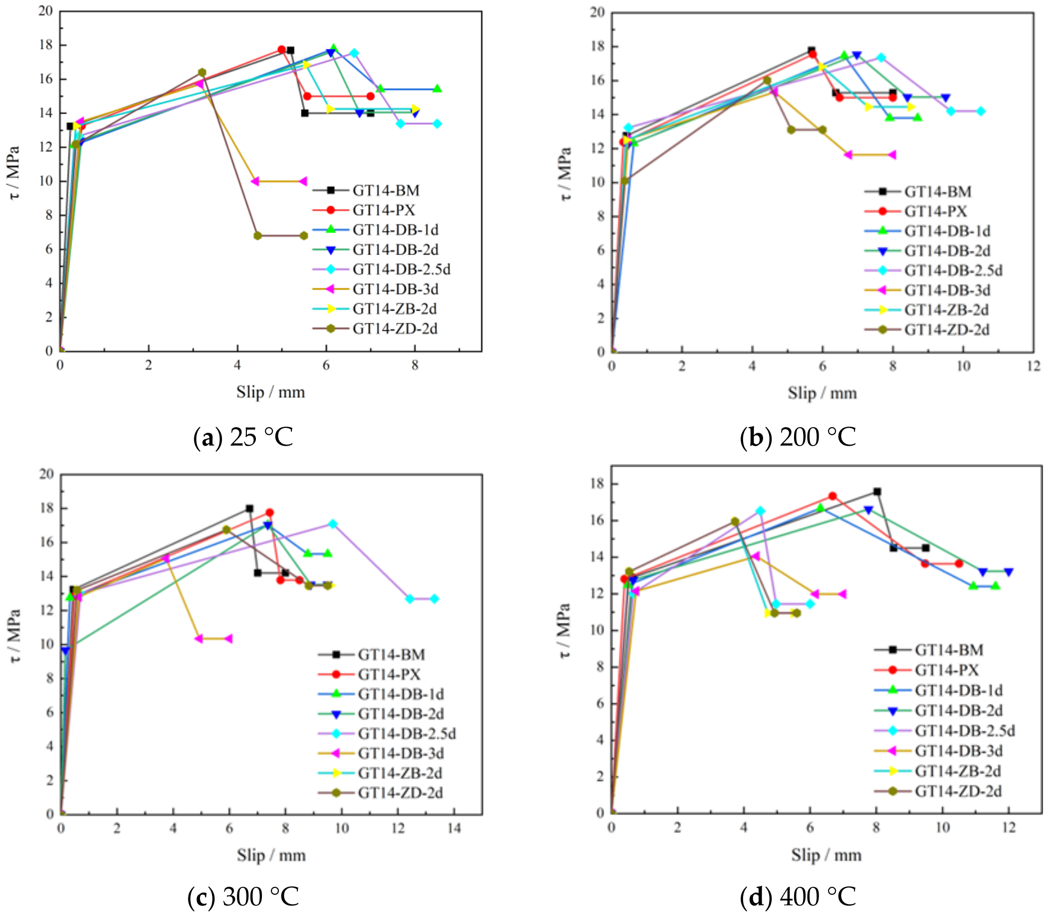

(**a**) 25 °C (**b**) 200 °C

(**c**) 300 °C (**d**) 400 °C

Figure 17. *Cont.*

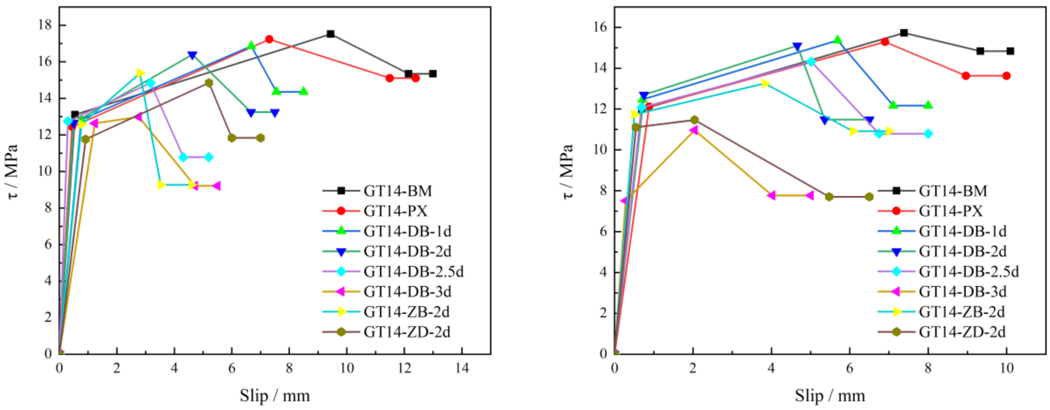

(**e**) 500 °C (**f**) 600 °C

Figure 17. Bond stress-slip curves under different temperatures.

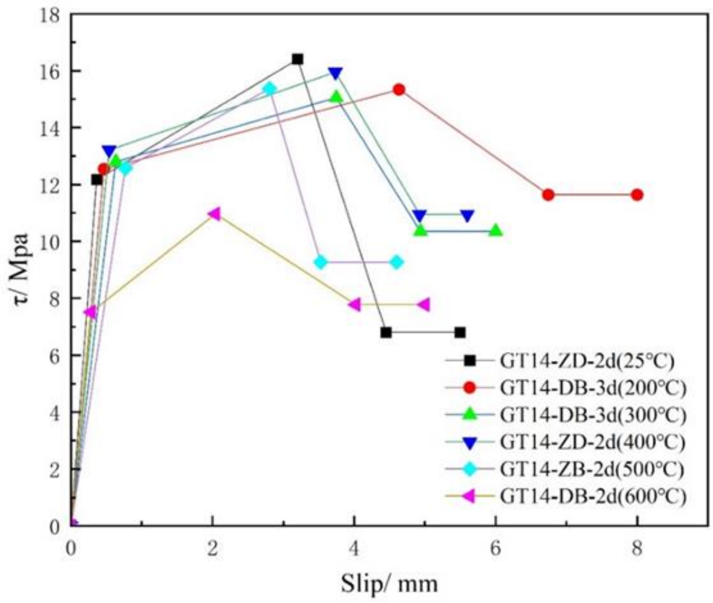

Figure 18. The most unfavorable bond stress-slip curves under different temperatures.

The failure modes were mainly rebar fracture failure and rebar pulled-out failure. The different failure modes are mainly determined by the bond strength between the rebar and the grout and the tensile capacity of the rebar. The impact of high temperature and defects on the bearing capacity of half-grouted sleeves is investigated through an analysis of the bond strength between the rebar and grout. The slip was monitored via an extensometer throughout the whole process, which is the relative sliding distance between the rebar and the grout at the grout end.

The relationship between the average bond stress and peak load is:

$$\tau = \frac{P_u}{\pi l d} \tag{7}$$

where P_u is the peak load under different temperatures, N; d is the diameter of rebar, mm; l is the anchorage length of rebar at the grouting end of the sleeve, mm, which is 120 mm in this test.

By calculating the bond stress of the half-grouted sleeve, the bond stress-slip curve of each specimen can be obtained, which should be similar to the trend of the load-slip curve. It can be roughly divided into four sections: micro-slip section, sliding section, descending section and residual section. The micro-slip bond stress corresponding to the end point of the micro-slip section is τ_s, and the corresponding slip amount is Ss. The maximum point corresponds to the ultimate bond stress τ_u, and the corresponding slip quantity is S_u. The splitting bond strength corresponding to the end point of the descending section is τ_r and the corresponding slip amount is S_r. The cohesive slip constitutive model of the half-grouted sleeve connector described by the four-stage formula is as follows, and the formula is determined by Appendix C: constitutive relationship of reinforced concrete and multiaxial strength criterion of concrete in gb50010-2010 [38]. Among them, section C3 specifies the proposal of this formula and the selection of parameters:

$$\tau = \begin{cases} \mathrm{k}\cdot \mathrm{s},\ 0 < \mathrm{s} < s_u \\ \mathrm{as} + \mathrm{b},\ \mathrm{s_s} < s < s_u \\ \mathrm{cs} + \mathrm{d},\ \mathrm{s_u} < s < s_r \\ \tau_{\mathrm{r}},\ \mathrm{s} > s_r \end{cases} \tag{8}$$

$$k = \frac{\tau_s}{s_s} \tag{9}$$

$$a = \frac{\tau_u - \tau_s}{s_u - s_s} \tag{10}$$

$$b = \tau_u - \frac{\tau_u - \tau_s}{s_u - s_s} \cdot s_u \tag{11}$$

$$c = \frac{\tau_u - \tau_r}{s_u - s_r} \tag{12}$$

$$d = \tau_u - \frac{\tau_u - \tau_r}{s_u - s_r} \cdot s_u \tag{13}$$

Combined with the grey correlation analysis and the trend of the two coefficient factors, it can be seen that the performance of the component has decreased significantly before and after 400 °C. With the increase in temperature to 400 °C, the bearing capacity of the specimen began to decrease significantly. At this time, the temperature has a greater impact on the tensile properties of the specimen, and with the increase in temperature, the greater the defect length, the more obvious the impact of temperature on the tensile properties.

Due to the occurrence of an end defect which is marked as DB, the effective anchorage length of reinforcement becomes shorter, while the compressive strength of grouting material decreases due to high temperature. Therefore, with the increase in temperature, the greater the length of end defects, the lower the bearing capacity, and the easier the reinforcement is pulled out. The half-grouted sleeve specimen with middle defects is more prone to pull-out failure than the specimen with end defects. The reason is that the setting defects affect the force transfer effect between the grouting material and the reinforcement. For the specimen with the same total effective anchorage length, the farther the defect is from the sleeve end, the lower the bearing capacity is. When the length of defects is the same, the bearing capacity of discrete defects is lower than that of the concentrated defects. Due to the set defects, the grouting material is divided into multiple stress sections, and the force transmission path is discontinuous, which has a great impact on the bearing capacity of the specimen.

With the increase in temperature, the safety factor and ductility factor of non-defective and defective half-grouted sleeve specimens decrease, and the safety factor and ductility factor of defective specimens are always lower than those of the control group at each temperature. For the same end defect specimen, the larger the defect length, the lower the safety factor and ductility factor. The safety coefficient and ductility coefficient of the GT14-DB-3d specimen are the lowest and the most unreliable. The influence of high temperature and defects on the performance of the half-grouted sleeve cannot be ignored.

3.5. Real Situation Fitting and Performance Improvement

In the actual project site, after the single-sided welding between the post repair connecting reinforcement and the sleeve is completed, the reinforcement grouting material shall be filled around the weld. Moreover, it can be improved by replacing concrete to prevent the impact of high temperature and defects. For example, plastic waste (PW) as aggregate or fiber in cement mortar and concrete manufacturing can effectively enhance the concrete performance and mechanical strength. It can not only recycle PW to achieve the purpose of environmental protection, but also improve the crack resistance performance, so as to show good crack resistance and high temperature resistance in fire disaster [39]. Improving the curing specimens can also enhance the compressive strength of concrete [40].

When size requirements are proposed for the sleeve to meet engineering objectives, although the specimen meets the specifications, improvements can still be made to expand the application range when considering size effects. When size requirements are proposed for the sleeve to meet engineering objectives, although the specimen meets the specifications, improvements can still be made to expand the application range when considering size effects. When studying the column base joint specifications of inverted exposed grooved slopes (IEGSs), the bearing capacity of the specimens can be improved by increasing the cross-sectional size of the columns, or by using cement-based grouting materials instead of concrete, which can increase the yield load and peak load by 9.97% and 6.31% [41].

4. Conclusions

A total of 48 half-grouted sleeve specimens were subjected to unidirectional tensile testing to investigate the post-fire mechanical properties of sleeve connectors with various grouting defects. Specimens were exposed to temperatures ranging from 25 °C to 600 °C. Grouting defects included end defects, middle defects, combined middle and end defects, and eccentric defects. Based on the analysis of the test results, the following conclusions can be drawn:

(1) The primary failure modes observed in the half-grouted sleeve specimens are rebar fracture failure and rebar pull-out failure. Upon reaching temperatures of 500 °C for non-defective specimens or exceeding 400 °C for defective specimens, a significant deterioration in the tensile properties of the half-grouted sleeve is evident, leading to a universal occurrence of rebar pull-out failure across all specimens.

(2) When the temperature reaches 400 °C, all the defect groups with reduced anchorage length fail. Different types of defects have different effects on mechanical properties of half-grouted sleeve specimens. The 3d defect at the end has the greatest influence on the tensile properties of the half-grouted sleeve connection. When the end defect length reaches 35 mm, because the defect length is too large, the anchorage length decreases, and the cementation force between the reinforcement and the grouting material is far less than the ultimate tensile strength of the reinforcement, the specimen is not reliable at normal temperature. The influence degree of different defects is greater than that of temperature.

(3) The ultimate tensile force, yield tensile force, safety factor and ductility factor of half-grouted sleeves with or without grouting defects decrease with increases in temperature. The rate of increase or decrease of these parameters varies depending on the type of defect. High temperatures and construction defect have important influence on the reliability of half-grouted sleeve connections. The defects have greater influence on it through the grey correlation analysis. The practical engineering significance provided in this experiment is as follows: considering that defects cannot be avoided during the production and construction process, it is necessary to increase the thickness of the protective layer of the wall while reducing defects to improve fire-resistance performance, so as to control the indoor temperature within 400 degrees Celsius as much as possible after a fire occurs.

(4) The use of advanced grouting materials or concrete can effectively improve the anti-cracking performance of time. When the conclusion is extended to full-size specimens,

considering the size effect, the bearing capacity of specimens can be improved by increasing the section size of columns or using cement-based grouting materials instead of concrete.

(5) For half-grouted sleeve connectors with the same total defect lengths, discrete defects result in lower bearing capacity compared to concentrate defects, and when defects are farther away from the sleeve end, the bearing capacity is lower. GT14-DB-2d has the best performance, followed by GT14-ZB-2d, and GT14-ZD-2d has the worst properties.

(6) Taking 400 °C as the critical point, high temperature has a significant impact on the stress of the half-grouted sleeve component after fire, so it is necessary to strengthen and improve the high temperature damage resistance of the half-grouted sleeve. By comparing the ultimate strength of the half-grouted sleeve with different thicknesses of the protective layer at different temperatures, it can be found that the ultimate strength and displacement of the specimen with the protective layer increase significantly, indicating that the appropriate increase in the thickness of the protective layer can effectively improve the ultimate strength of the half-grouted sleeve. In addition, the increase in anchorage length can also effectively improve the fire resistance of the connecting part.

On the basis of this research, the numerical simulation of the half-grouted sleeve with grouting defects after fire is carried out. This research serves as a valuable foundation for subsequent studies on simulation models. For example, the mechanical analysis of specimens under high stress and large deformation repeated tension and compression after high temperature can be further studied. The stress–strain relationship of grouting material can also be further explored, as well as the grouting material in line with the actual situation.

Author Contributions: Conceptualization, S.H. and D.C.; methodology, S.H., T.X. and D.C.; software, S.J.; formal analysis, D.C., S.H. and S.J.; writing—original draft preparation, S.J. and H.L.; writing—review and editing, S.J., D.C., H.L. and T.X.; resources, T.X. All authors have read and agreed to the published version of the manuscript.

Funding: This work was supported by Anhui University Natural Science Research Project (KJ2021A0608) and Young and middle-aged teachers training action discipline (professional) leader training project (DTR2023028) and Science and Technology Project of Anhui Province Housing and Urban–Rural Construction (2020-YF47).

Data Availability Statement: For privacy reasons, the data presented in this article are available only on reasonable request from the corresponding author.

Conflicts of Interest: Author Shouying Hu was employed by the company A+E Design Co., Ltd. Shenzhen 518031, China. Author Tao Xu was employed by the company China Construction First Group the Fifth Construction Co., Ltd. The remaining authors declare that the research was conducted in the absence of any commercial or financial relationships that could be construed as a potential conflict of interest.

References

1. Che, W.P.; Chen, J.W.; Liu, Z.Y.; Tian, W.L. Mechanical properties of cast half-grouted sleeve splice with rebar bonding defects. *Adv. Struct. Eng.* **2022**, *25*, 2870–2884. [CrossRef]
2. Zhao, C.F.; Zhang, Z.D.; Wang, J.F.; Wang, B. Numerical and theoretical analysis on the mechanical properties of improved CP-GFRP splice sleeve. *Thin-Walled Struct.* **2019**, *137*, 487–501. [CrossRef]
3. Xu, L.; Pan, J.L.; Cai, J.M. Seismic performance of precast RC and RC/ECC composite columns with grouted sleeve connections. *Eng. Struct.* **2019**, *188*, 104–110. [CrossRef]
4. Han, Q.; Li, X.P.; Xu, K.; Lu, Y.Q.; Du, X.L.; Wang, Z.Q. Shear strength and cracking mechanism of precast bridge columns with grouted sleeve connections. *Eng. Struct.* **2021**, *230*, 111616. [CrossRef]
5. Liu, H.T.; Chen, J.N.; Xu, C.S.; Du, X.L. Seismic performance of precast column connected with grouted sleeve connectors. *J. Build. Eng.* **2020**, *31*, 101410. [CrossRef]
6. Tang, H.S.; Xie, Y.J.; Zhao, T.T.; Xue, S.T. Identification of Grout Sleeve Joint Defect in Prefabricated Structures Using Deep Learning. *Front. Mater.* **2020**, *7*, 298. [CrossRef]

7. Liu, Q.Z.; Li, J.Z.; Li, M.F.; Wu, X.K.; Li, Y.C.; Zhang, L. Bond performance prediction model of defective grout in post-fire sleeve connections under cyclic loading. *Constr. Build. Mater.* **2023**, *400*, 132442. [CrossRef]
8. Li, Y.B.; Cheng, L.; Lei, W.Y.; Su, Y.; Huang, T.; Zhu, Y.X.; Mei, C.; He, X.Y. Microstructures and mechanical property of post-fire grouting sleeve connections considering concrete cover. *Constr. Build. Mater.* **2023**, *403*, 132578. [CrossRef]
9. Gao, Q.; Zhao, W.J. Experimental study on factors influencing the connection performance of grouted welded sleeves under uniaxial tensile loads. *J. Build. Eng.* **2021**, *43*, 103033. [CrossRef]
10. Huang, Y.; Zhu, Z.G.; Naito, C.J.; Yi, W.J. Tensile behavior of half grouted sleeve connections: Experimental study and analytical modeling. *Constr. Build. Mater.* **2017**, *152*, 96–104.
11. Yu, Q.; JQ, S.; WH, Y. Experimental study on bond behavior between ribbed steel bars and sleeve constrained grouting material. *J. Harbin Inst. Technol.* **2018**, *50*, 98–106.
12. Liu, C.; Pan, L.F.; Liu, H.; Tong, H.W.; Yang, Y.B.; Chen, W. Experimental and numerical investigation on mechanical properties of grouted-sleeve splices. *Constr. Build. Mater.* **2020**, *260*, 120441. [CrossRef]
13. Guo, H.; Zhang, J.; Wang, C. Experimental study on influence of connection defects on joint strength of half-grouted sleeve splicing of rebar. *Adv. Civ. Eng.* **2020**, *2020*, 5389861. [CrossRef]
14. Chen, J.W.; Wang, Z.W.; Liu, Z.Y.; Ju, S.L. Experimental investigation of mechanical behaviour of rebar in steel half-grouted sleeve connections with defects in water/binder ratio. *Structures* **2020**, *26*, 487–500. [CrossRef]
15. Zhang, X.; Zhao, Y.H.; Guo, Y.F.; Li, Z.Y. Equivalent stress-strain model of half grouted sleeve connection under monotonic and repeated loads: Experiment and preliminary application. *Eng. Struct.* **2022**, *260*, 114247. [CrossRef]
16. Zheng, G.Y.; Kuang, Z.P.; Xiao, J.Z.; Pan, Z.F. Mechanical performance for defective and repaired grouted sleeve connections under uniaxial and cyclic loadings. *Constr. Build. Mater.* **2020**, *233*, 117233. [CrossRef]
17. Xu, F.; Wang, K.; Wang, S.G.; Li, W.W.; Liu, W.Q.; Du, D.S. Experimental bond behavior of deformed rebars in half-grouted sleeve connections with insufficient grouting defect. *Constr. Build. Mater.* **2018**, *185*, 264–274. [CrossRef]
18. Kahama, E.K.; Xie, F.Z.; Anglaaere, D.L.M. Numerical study on the influence of defects in grouting on the mechanical properties of a full grouted sleeve connector. *J. Adhes.* **2022**, *98*, 2550–2581. [CrossRef]
19. Zheng, Q.L.; Wang, N.; Tao, L.; Xu, W.J. Experimental study on effects of grout defects on the connection behaviors of grout sleeve splicing for reinforcing bars. *Build. Sci.* **2017**, *33*, 61–68.
20. Xie, L.; Wang, X.; Yang, C.; Jiang, Y.; Liu, Q.; Miao, Q.; Chen, X. Development and validation of a defect detection and repair method for half grouted sleeve connection. *Case Stud. Constr. Mater.* **2022**, *17*, e01205. [CrossRef]
21. Chen, H.B.; Zhou, J.C. Experimental study on mechanical properties of sleeve grouting material after fire. *J. Saf. Sci. Technol.* **2022**, *18*, 145–151.
22. Zhang, W.X.; Deng, X.; Zhang, J.Y.; Yi, W.J. Tensile behavior of half grouted sleeve connection at elevated temperatures. *Constr. Build. Mater.* **2018**, *176*, 259–270. [CrossRef]
23. Zhu, J.N.; Ma, J.F.; Guo, D.D.; Wu, Y.P.; Ma, J.J. Study on tensile properties of semi grouted sleeve connectors after high temperature. *Constr. Build. Mater.* **2021**, *302*, 124088. [CrossRef]
24. Zhang, W.X.; Lv, W.L.; Zhang, J.Y.; He, C.; Deng, X.; Yi, W.J. Post-fire tensile properties of half-grouted sleeve connection under different cooling paths. *Fire Saf. J.* **2019**, *109*, 102848. [CrossRef]
25. Wang, T.; Xu, H.M.; Yu, M.; Xu, L.H.; Ye, J.Q. Experimental investigation on the failure modes of grouted sleeve connections under thermal and mechanical loads. *Eng. Fail. Anal.* **2020**, *109*, 104246. [CrossRef]
26. Wang, T.; Yu, M.; Li, X.Y.; Yan, Z.G.; Saafi, M.; Ye, J.Q. Experimental investigation on the post-fire cyclic behavior of grouted sleeve connections. *Constr. Build. Mater.* **2021**, *279*, 122394. [CrossRef]
27. Xiao, J.Z.; Liu, L.L.; Ding, T.; Xie, Q.H. Experimental study on mechanical behavior of thermally damaged grouted sleeve splice under cyclic loading. *Struct. Concr.* **2020**, *21*, 2494–2514. [CrossRef]
28. Zhang, W.X.; He, C.; Zhang, J.Y.; Yi, W.J.; Deng, X. Mechanical behavior of post-fire half-grouted sleeve connection covered by concrete. *Constr. Build. Mater.* **2019**, *201*, 218–231. [CrossRef]
29. *JG/T408-2019*; Cementitious Grout for Sleeve of Rebar Splicing. Architecture & Building Press: Beijing, China, 2019.
30. *JGJ 107-2016*; Technical Specification for Mechanical Splicing of Steel Reinforcing Bars. Architecture & Building Press: Beijing, China, 2016.
31. *GB/T 2419-2005*; Test method for fluidity of cement mortar. National Standards of the People's Republic of China: Beijing, China, 2005.
32. *GBT 50448-2015*; Technical Code for Application of Cementitious Grout. Architecture & Building Press: Beijing, China, 2015.
33. *GB/T228.1-2021*; Metallic Materials-Tensile Testing-Part 1: Method of Test at Room Temperature. Architecture & Building Press: Beijing, China, 2022.
34. *JGJ355-2015*; Technical Specification for Grout Sleeve Splicing of Rebars. Architecture & Building Press: Beijing, China, 2015.
35. Lin, F.; Wu, X.B. Effect of sleeve length on deformation properties of grouted splices. *Gradevinar* **2017**, *69*, 537–546.
36. Guo, T.; Yang, J.; Wang, W.; Li, C. Experimental investigation on connection performance of fully-grouted sleeve connectors with various grouting defects. *Constr. Build. Mater.* **2022**, *327*, 126981. [CrossRef]
37. Zhang, K. *Experimental Investigation on the Residual Mechanical Properties of FRP Bars in the Structure during and after Exposure to High Temperatures*; Southeast University: Nanjing, China, 2019; pp. 68–76.

38. *gb50010-2010*; Appendix C: Constitutive Relationship of reinforced concrete and Multiaxial Strength Criterion of Concrete. Code for Design of Concrete Structures. Architecture & Building Press: Beijing, China, 2005.
39. Ahmad, J.; Majdi, A.; Elhag, A.B.; Deifalla, A.F.; Soomro, M.; Isleem, H.F.; Qaidi, S. A Step towards Sustainable Concrete with Substitution of Plastic Waste in Concrete: Overview on Mechanical, Durability and Microstructure Analysis. *Crystals* **2022**, *12*, 944. [CrossRef]
40. Jaf, D.K.I.; Abdulrahman, P.I.; Mohammed, A.S.; Kurda, R.; Qaidi, S.M.A.; Asteris, P.G. Machine learning techniques and multi-scale models to evaluate the impact of silicon dioxide (SiO_2) and calcium oxide (CaO) in fly ash on the compressive strength of green concrete. *Constr. Build. Mater.* **2023**, *400*, 132604.
41. Qiao, D.H.; Xu, Y.Q.; Zhang, X.; Pang, J.B.; Liu, K.; Wang, S.J. Seismic behaviour and size effect of column base joints with inverted exposed grouted sleeves. *J. Build. Eng.* **2022**, *51*, 104333. [CrossRef]